Detection of organic carbon in Mars-analog paleosols with thermal and evolved gas analysis

Adrian P. Broz* [1,] Joanna Clark[2], Brad Sutter[3], Doug W. Ming[4], Briony Horgan[5], Paul Douglas Archer[3] and Lucas C.R. Silva[6,7]

[1]Department of Earth Sciences, University of Oregon, Eugene, OR 97405

[2] Geocontrols Systems – Jacobs JETS Contract, NASA Johnson Space Center, Houston, TX, 77058

[3] Jacobs JETS Contract, NASA Johnson Space Center, Houston, TX 77058

[4]NASA Johnson Space Center, Houston, TX, 77058

[5]Department of Earth, Atmospheric and Planetary Science, Purdue University, IN, 47907

[6] Environmental Studies Program, Department of Geography, University of Oregon, Eugene, OR 97405

[7] Institute of Ecology and Evolution, University of Oregon, Eugene, OR 97405

*Corresponding author, abroz@uoregon.edu

21

Detection of organic carbon in Mars-analog paleosols with thermal and evolved gas analysis

24

25

Adrian P. Broz* [1,] Joanna Clark[2], Brad Sutter[3], Doug W. Ming[4], Briony Horgan[5], Paul Douglas Archer[3] and Lucas C.R. Silva[6,7]

[1]Department of Earth Sciences, University of Oregon, Eugene, OR 97405

[2] Geocontrols Systems – Jacobs JETS Contract, NASA Johnson Space Center, Houston, TX, 77058

[3] Jacobs JETS Contract, NASA Johnson Space Center, Houston, TX 77058

[4]NASA Johnson Space Center, Houston, TX, 77058

[5]Department of Earth, Atmospheric and Planetary Science, Purdue University, IN, 47907

[6] Environmental Studies Program, Department of Geography, University of Oregon, Eugene, OR 97405

[7] Institute of Ecology and Evolution, University of Oregon, Eugene, OR 97405

*Corresponding author, abroz@uoregon.edu

36

Abstract

Decades of space exploration have shown that surface environments on Mars were habitable billions of years ago. Ancient, buried surface environments, or paleosols, may have been preserved in the geological record on Mars, and are considered high-priority targets for biosignature investigation. Studies of paleosols on Earth that are compositionally similar to putative martian paleosols can provide a reference frame for constraining their organic preservation potential on Mars. However, terrestrial paleosols typically preserve only trace amounts of organic carbon, and it remains unclear whether the organic component of paleosols can be detected with Mars rover-like instruments. Furthermore, the study of terrestrial paleosols is complicated by diagenetic additions of organic carbon, which can confound interpretations of their organic preservation potential. The objectives of this study were a) to determine whether organic carbon in ~30-million-year-old Mars-analog paleosols can be detected with thermal and evolved gas analysis, and b) constrain the age of organic carbon using radiocarbon (^{14}C) dating to identify late diagenetic additions of carbon. Al/ Fe smectite-rich paleosols from the Early Oligocene (33 Ma) John Day Formation in eastern Oregon were examined with a thermal and evolved gas analyzer configured to operate similarly to the Sample Analysis at Mars Evolved Gas Analysis (SAM-EGA) instrument onboard the Mars Science Laboratory *Curiosity* rover. All samples evolved CO_2 with peaks at ~400 °C and ~700° C from the thermal decomposition of refractory organic carbon and small amounts of calcium carbonate, respectively. Evolutions of organic fragments co-occurred with evolutions of CO_2 from organic carbon decomposition. Total organic carbon (TOC) ranged from 0.002 - 0.032 ±

57 **0.006 wt. %. Like modern soils, the near-surface horizons of all paleosols had significantly higher**
58 **TOC relative to subsurface layers. Radiocarbon dating of four samples revealed an organic carbon**
59 **age ranging between ~6,200 – 14,500 years before present, suggesting there had been inputs of**
60 **exogenous organic carbon during diagenesis. By contrast, refractory carbon detected with EGA**
61 **and enrichment of TOC in near-surface horizons of all three buried profiles were consistent with**
62 **the preservation of trace amounts of endogenous organic carbon. This work demonstrates that**
63 **near-surface horizons of putative martian paleosols should be considered high priority locations for**
64 *in-situ* **biosignature investigation and reveals challenges for examining organic matter preservation**
65 **in terrestrial paleosols.**

1. Introduction

67   Paleosols are ancient, buried soils that are commonly lithified into sedimentary rocks. Terrestrial
68 paleosols are a geological record of the atmospheric composition, climate, topography and organisms
69 present before soil burial [1]. On Mars, paleosols may have formed in sediments such as basaltic sand or
70 volcanic ash that were subject to subaerial weathering by surface waters [2] and were subsequently buried
71 and preserved in the geological record. Orbital remote sensing of the global martian surface has detected
72 minerals within Noachian-age (4.1-3.7 Ga) layered sedimentary rocks that are consistent with
73 precipitation-driven pedogenic weathering of mafic sediments [3–5]. Noachian sedimentary rocks with
74 spectral signatures of subaerial weathering have been detected in thousands of locations across the surface
75 of Mars. One hypothesis is that these deposits are paleosols [3] which are the common products of
76 pedogenic alteration followed by burial. Mounting evidence of global-scale aqueous alteration of the
77 Martian surface during the Noachian [3,6] suggests that pedogenesis could have been a critical process early
78 in the planet's history. As such, paleosols have been recently named a high priority location for
79 biosignature investigation [7] and Mars Sample Return [8], but the biosignature preservation potential of
80 paleosols with Mars-like mineralogy remains poorly constrained [9].
81   On Earth, soils are highly habitable environments. Modern soils are teeming with microbial
82 biomass, often averaging 10^{10}–10^{11} bacterial cells and 10^3 and 10^4 species per gram of soil [10]. Modern
83 soils also contain more organic carbon than global vegetation and the atmosphere combined [11,12].
84 Similarly, Earth's oldest soils also appear to have been highly habitable environments. Many Precambrian
85 (> 541 Ma) paleosols contain organic carbon and other chemical biosignatures that are thought to be
86 remnants of surface biomass [13–16]. Furthermore, Archean (> 2 Ga) paleosols contain filamentous organic
87 carbon and organo-mineral complexes possibly derived from cyanobacterial mats on the soil surface [17,18].
88   Many terrestrial paleosols preserve only trace amounts of organic carbon, especially compared to
89 modern soils, marine shales, and lacustrine rocks [1]. Organic carbon losses during diagenesis can reduce
90 the organic carbon content of paleosols by up to two orders of magnitude relative to their modern soil
91 counterparts [13]. Severe losses of organic carbon are most common in paleosols that originally formed
92 under oxidizing, well-drained conditions [19]. In general, oxidized paleosols typically contain only low
93 amounts (< 0.1 wt. %) of organic carbon [13]. Diagenetic losses of organic carbon in oxidized terrestrial
94 paleosols poses major challenges for detection of chemical and isotopic biosignatures preserved within
95 the organic matter fraction. However, this is not the case for all paleosols. Those that originally formed
96 under reducing conditions, such as Permian (~250 Ma) Histosols (poorly drained organic soils), preserve
97 organic carbon with abundances > 25 wt. % [20], implying that redox state before burial may provide a first-
98 order control on the preservation of organic carbon in ancient soils [21].

99   An additional concern for the study of terrestrial paleosol organic matter is that diagenetic
100   alterations ranging from groundwater alteration to precipitation-driven leaching of dissolved organic
101   carbon can result in the addition of exogenous organic molecules, so caution is necessary for interpreting
102   whether the organic fraction has indeed been "preserved" over geological time scales. In other words,
103   terrestrial paleosols can be contaminated by organic molecules that were not original to the soil, thereby
104   complicating efforts to interpret their biosignature preservation potential.
105   One way to constrain the biosignature preservation potential of putative paleosols on Mars is to
106   examine the organic fraction of paleosols from Earth that share compositional and morphological
107   similarities to layered sedimentary rocks on Mars. Examination of oxidized paleosols with Mars-like
108   mineralogy can help determine if low amounts of organic molecules within natural pedogenic mineral
109   matrices can be detected with Mars flight-analog instruments. Furthermore, cosmogenic nuclide dating of
110   these analog paleosols can also identify potential diagenetic additions of organic carbon.
111   This study builds on and combines previous results from an established Mars-analog paleosol
112   sequence (**Broz et al, 2021, in review).** The focus here is to determine if organic molecules in oxidized
113   paleosols are detectable with Mars flight-analog instrumentation, and to determine if there have been
114   post-depositional additions of exogenous organic carbon. The objectives of this study were a) to
115   determine whether organic carbon in ~30-million-year-old Mars-analog paleosols can be detected with
116   thermal and evolved gas analysis, and b) constrain the age of organic carbon using radiocarbon (^{14}C)
117   dating to identify late diagenetic additions of carbon.
118
119   1.1 Paleosols at John Day Fossil Beds National Monument in eastern Oregon, USA
120   Eocene and Oligocene (42-28 Ma) sedimentary rocks at John Day Fossil Beds National
121   Monument in eastern Oregon are a thick sequence of volcaniclastic paleosols which altogether span over
122   400 meters of vertical stratigraphy. [22–25]. The paleosol sequence contains over 500 clay mineral-rich (30-
123   95 wt. %) paleosols formed over ~15 Myr through the Eocene-Oligocene boundary (Figure 1) [23,26]. Each
124   of the individual profiles formed from pedogenic alteration of andesitic to rhyodacitic volcanic ash and/or
125   tuff, followed by rapid burial via emplacement of an additional layer of tephra onto the soil surface. This
126   process of soil formation and burial repeated for nearly 15 million years, and as such, the paleosol
127   sequence provides a unique record of Cenozoic climate change in eastern Oregon. Changes in mineralogy
128   throughout the paleosol sequence reflect the Eocene-Oligocene cooling and drying of the climate [27].
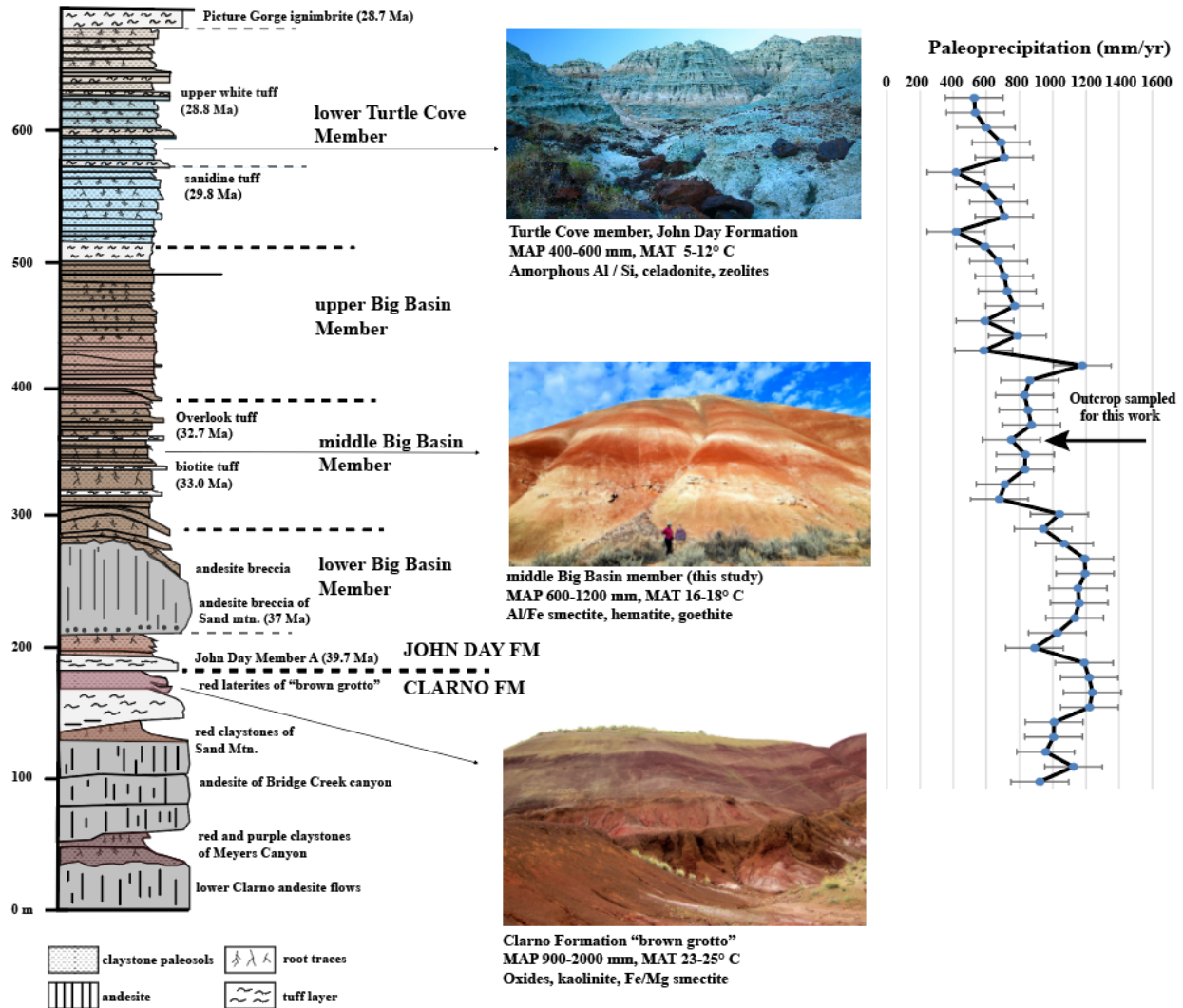
Figure 1. A sequence of Eocene and Oligocene (42-28 Ma) volcaniclastic paleosols in the Clarno and John Day Formations, John Day Fossil Beds National Monument (after [22] and [28]). Declining precipitation through the Eocene/Oligocene boundary is inferred from the mineralogy of paleosols from the Clarno and John Day Formations. Paleoprecipitation estimates are from [28] who used an equation relating molecular weathering ratios (Bases/alumina $[CaO + MgO + Na_2O + K_2O / Al_2O_3]$ to mean annual precipitation from a database of modern U.S soils (r=0.79, standard error = 179 mm). The stratigraphic level of paleosols analyzed in this work are indicated (black arrow, far right).

The Eocene (42-39 Ma) Clarno Formation represents the lowest and oldest unit of the Oregon paleosol sequence. The basal Clarno Formation is characterized by andesite flows interspaced with severely weathered paleosols with accumulations of kaolinite, Fe/Mg smectite and oxides (Oxisols and Ultisols in US soil taxonomy) which indicate tropical weathering conditions in the middle to late Eocene [23]. A particularly striking exposure of the late Eocene Clarno Formation at the "Brown Grotto" area of the Painted Hills is characterized by thick (~2-6 meter), repeated profiles of deeply weathered lateritic paleosols (Figure 1, bottom) that are similar to modern soils from Southern Mexico and Central America in climates that are subtropical and humid [23]. Stratigraphically above the Clarno Formation, the early Oligocene (~33 Ma) Big Basin Member of the John Day Formation is characterized by less intensely

147 weathered paleosols (Alfisols and Inceptisols) that are rich in Al and Fe smectites such as nontronite and
148 montmorillonite (Figure 1, middle). This middle unit represents a dramatic cooling and drying of the
149 climate through the Eocene-Oligocene boundary. Overlying this unit of the paleosol sequence is the mid-
150 late Oligocene (~28 Ma) Turtle Cove Member of the John Day Formation (Figure 1, top). The brown,
151 green and celadon-colored paleosols of this unit are minimally weathered Aridisols (desert soils) and
152 Andisols (amorphous-rich volcanic soils). Paleosols in this unit are characterized by accumulations of
153 amorphous and nanocrystalline materials (e.g., allophane and imogolite), pedogenic calcite, and
154 diagenetic celadonite [24]. There is a dramatic reduction in smectite content and absence of kaolinite which
155 is consistent with weathering under a semi-arid to arid climate regime [27]. Finally, the entire paleosol
156 sequence is capped by approximately 300 vertical meters of flood basalts from the Miocene (~16 Ma)
157 Columbia River Basalt Group. Based on these mineralogical transitions, the Eocene paleosols with
158 accumulations of kaolinite and oxides appear to reflect a subtropical and humid climate, while
159 accumulations of nanophase aluminosilicates and amorphous phases in overlying paleosols indicate
160 stepwise and cooling and drying during the late Oligocene [23].
161
162 **1.2 Pedogenic weathering on early Mars and comparisons to terrestrial paleosols**
163
164   From a global perspective, orbital remote sensing from Observatoire pour la Minéralogie, l'Eau,
165 les Glaces, et l'Activité (OMEGA) and the Compact Reconnaissance Spectrometer at Mars (CRISM)
166 instrument onboard the Mars Reconnaissance Orbiter provide the most compelling evidence of extensive
167 pedogenic-like alteration across the surface of Mars. Potential weathering sequences have been detected
168 in hundreds of locations across Noachian-age terrains, wherever these ancient rocks are not obscured by
169 dust, sand, or overlying strata [3,4]. OMEGA and CRISM have collectively gathered visible and near-
170 infrared (VNIR) reflectance spectra of sedimentary deposits at Mawrth Vallis, Oxia Planum, Nili Fossae
171 and other altered Noachian terrains. Some of these deposits, such as layered outcrops at Mawrth Vallis,
172 have spectral and stratigraphic similarities to terrestrial paleosol sequences [24,26,29–31]. Spectral refinements
173 for CRISM images (e.g., [32]) are allowing for identification of smaller-scale hydrated mineral deposits at
174 Mawrth Vallis that facilitate a detailed reconstruction of possible geochemical environments on early
175 Mars [33].
176
177 **Mawrth Vallis**
178   Previous work identified compositional and morphological similarities between the eastern
179 Oregon paleosol sequence and layered outcrops at Mawrth Vallis [24,29,34,35]. The compositional stratigraphy
180 at Mawrth Vallis has been interpreted as a paleosol sequence [24] or a deep weathering profile [6]. Here, a
181 ~200 m stack of layered sedimentary rocks has spectral signatures consistent with pedogenic-like
182 alteration of mafic sediments[36]. The basal Fe/Mg smectite unit at Mawrth Vallis is dominated by spectral
183 signatures of Fe/Mg smectite and is consistent with subaerial alteration under a warm and wet climate
184 [31,37]. This basal unit transitions upward into a thin, ferrous-bearing clay unit that could have resulted from
185 reducing conditions during subaerial weathering. This unit is overlain by layered rocks containing
186 minerals consistent with formation in acidic and evaporitic geochemical settings, inferred from spectral
187 signatures consistent with mixtures of smectite and jarosite (the "doublet' spectral feature) [33,38,39].
188 Stratigraphically higher, layered rocks with signatures of Al and Fe smectite are consistent with
189 pedogenic weathering of volcaniclastic sediments under a semi-arid climate. Finally, the uppermost layers
190 are characterized by accumulations of poorly consistent aluminosilicates, suggesting minimal or cool-

191 climate alteration, which may represent the terminus of warm and wet conditions on early Mars [33]. The
192 entire sequence is then capped by dark-toned sands and/or lava flows. One hypothesis to explain the
193 stratigraphy at Mawrth Vallis is that it may represent the cooling and drying of the Martian climate during
194 the mid to late Noachian [33,40]. Similarly, the Oregon paleosol sequence represents a transition from warm
195 and wet conditions. The intensely weathered basal Clarno Formation paleosols transition upward into
196 less-weathered semi-arid paleosols of the middle Big Basin Member, which contains both oxidized (red,
197 brown) and reduced (yellow, black) paleosols. These are subsequently overlain by minimally weathered
198 paleosols of the Oligocene Turtle Cove Member with accumulations of unweathered volcanic glass,
199 amorphous colloids, calcite and hydrated silica which are thought to represent the terminus of warm and
200 wet climate conditions in eastern Oregon. Terrestrial paleosols at the analog site have therefore been
201 considered analogous to dioctahedral clay sequences on Mars. Layered rocks at Mawrth Vallis currently
202 stand as the best example of a putative paleosol sequence on Mars, but other locations, such as Jezero
203 Crater, also show VNIR spectra consistent with subaerial alteration of mafic sediments.
204
205 **Jezero Crater**
206   Spectral signatures of Al-bearing clay minerals and/or silica deposits that could have formed in
207 subaerial environments were detected approximately 3 km from the Perseverance rover landing site at
208 Jezero Crater. Across Jezero's western delta and northern fans, there are strong and ubiquitous orbital
209 detections of Al-bearing clay minerals and/or silica that could be either detrital or authigenic in origin [41].
210 The strongest signatures across the western delta are associated with features that resemble point bar
211 deposits and are consistent with formation in subaerial and/or seasonally waterlogged paleoenvironments
212 [41]. If authigenic in origin, these deposits could be subaerial paleoenvironments and include individual
213 paleosol profiles. If targeted for *in-situ* examination by *Perseverance* rover, these deposits could provide
214 critical information about the climate and duration of delta activity at Jezero Crater [41]. Similarly,
215 terrestrial paleosols examined in this study formed from subaerial weathering of volcaniclastic sediments
216 across alluvial terraces and have accumulated abundant Al clay minerals and amorphous silica [22,23]. The
217 mounting evidence of pedogenic-like processes on Mars emphasizes the need for study of paleosols from
218 Earth to aid in future investigation and interpretation of sedimentary rocks on Mars.
219
220 **Terrestrial paleosols: Mineralogy and diagenesis**
221   The present study focuses on three paleosol profiles from the early Oligocene (33 Ma) Big Basin
222 Member of the John Day Formation (Figure 1, middle). A detailed analysis of mineralogy and diagenetic
223 alteration of samples taken from paleosol profiles was previously performed **(Broz et al, 2021, in**
224 **review)**. X-ray diffraction evolved gas analysis and visible-near-infrared spectroscopy revealed high
225 abundances (> 80 wt. %) of montmorillonite and nontronite with lesser amounts of hematite, zeolites,
226 gypsum, and hydrated silica. Diagenetic alterations previously observed in these samples included a)
227 "burial gleization" of near-surface horizons, e.g., microbial reduction of Fe^{3+} in near-surface horizons of
228 paleosols, possibly during anaerobic decay of organic matter; b) dehydration of ferrous oxyhydroxides
229 (goethite) to form fine-grained hematite; c) zeolitization to form clinoptilolite, possibly resulting from
230 diagenetic recrystallization of a poorly crystalline smectite; and d) significant mechanical compaction to
231 approximately 70% of the original soil thickness **(Broz et al., 2021, in review).**
232   Previously, there was no effort to examine the organic component of these paleosols, and the
233 resulting influence of diagenesis on the organic fraction of Mars-analog paleosols is poorly understood.
234 Examination of terrestrial paleosols with Mars flight-analog instruments such as evolved gas analysis

235 allows for a detailed characterization of the organic fraction (discussed below). This can help ascertain if
236 diagenesis has resulted in severe losses of organic carbon in Mars-analog paleosols, and determine if
237 organic carbon that remains is detectable with analytical techniques relevant to Mars exploration.
238
239 **1.3 Sample Analysis at Mars (SAM) instrument onboard *Curiosity* Mars Rover**
240 The overall goal of the SAM instrument was to assess the potential for past habitability by
241 characterizing the martian chemical and isotopic composition of the atmosphere and volatile-bearing
242 surface materials [42]. The SAM instrument was integral in providing an understanding of organic materials
243 and phases undetectable by CheMin (e.g., amorphous phases, low abundance phases). SAM heats
244 scooped or drilled rock samples from ~30 – 870° C at 35° C min^{-1}. Evolved gases produced from the
245 thermal decomposition of volatile-bearing phases were analyzed by a quadrupole mass spectrometer
246 (QMS), gas chromatograph columns for GCMS, or a tunable laser spectrometer (TLS) [42]. In evolved gas
247 analysis (SAM-EGA) mode, SAM detected bulk gas evolution, whereas in gas chromatography-mass
248 spectroscopy (SAM-GCMS) mode, SAM performed molecular separation and identification of organic
249 molecules [42,43]. This study focused on SAM-EGA, so SAM-GCMS will not be further discussed. A
250 comprehensive discussion on how organic molecules are detected with SAM- GCMS mode can be found
251 in [42] and [44].
252 Evolved gases and their release temperatures detected by SAM-EGA provide constraints on the
253 mineralogy and organic content of samples in Gale Crater [43,45–47]. The thermal decomposition of solid
254 samples during SAM-EGA occurs during ramped heating, which releases volatile gases including CO_2,
255 CO, hydrocarbons, and organic fragments (i.e., CH_2, CH_3, C_2H_2 and others) that are detected by the QMS.
256 The intensity (relative abundance) of volatile release is plotted as a function of the release temperature,
257 generating a time and temperature series of data for each volatile gas release. The volatile release peak
258 temperature during sample decomposition depends on the thermodynamics of the reaction and can be
259 used to constrain the composition of minerals and organic carbon in the sample [45], as well as to identify
260 possible associations between minerals and organics [48].
261 Additional future missions to Mars will also employ EGA-like analysis to search for organic
262 molecules. The Mars Organic Molecule Analyzer (MOMA) onboard European Space Agency's ExoMars
263 2022 *Rosalind Franklin* rover will use pyrolysis gas chromatography-mass spectrometry (GCMS) and
264 laser desorption spectroscopy to search for biosignatures on Mars. Volatile gases thermally evolved from
265 solid samples in the instrument oven will be separated by the GC and then analyzed individually with the
266 MS [49] as is the case with SAM-GCMS, though MOMA will combine pyrolysis with laser desorption mass
267 spectrometry, a less destructive technique that allows for identification of large intact molecules and polar
268 compounds. The *Rosalind Franklin* rover will land at Noachian –age (3.9 Ga) Oxia Planum which
269 appears to be a westward extension of the lower parts of the stratigraphy observed at Mawrth Vallis [50,51].
270 Like Mawrth Vallis, strong and ubiquitous spectral signatures of dioctahedral Al-rich clay minerals
271 overlying Fe/ Mg clay minerals suggests Oxia Planum may host remnants of a thick (~200 m) deep
272 weathering profile or paleosol sequence that the rover could encounter during its primary mission.
273
274 **1.4 Previous detections of organic carbon with SAM-EGA**
275 Organic carbon has been detected in sedimentary rocks at Gale Crater with the SAM instrument
276 using both QMS and GCMS [44,46,47,52]. Abundances of reduced carbon were very low (< 1 wt. %) and
277 restricted to three samples (Cumberland [CB], Confidence Hills [CH], and Mojave [MJ]). Though all CO_2
278 and CO detected to date is consistent with oxidized organic compounds, it is possible that contamination

279   by the SAM-GCMS derivatization agent MTBSTFA could have resulted in these peaks. However, high-
280   temperature (> 600° C) CO releases were consistent with endogenous oxidized martian organics.
281   Additionally, chlorinated hydrocarbons (chlorobenzene [m/z 112], ~30 pmol) in the Cumberland drill
282   sample and organo-sulfur compounds including thiophenes and thiols (~90 nmol) in the Mojave and
283   Confidence Hills drill samples were identified in ~3.5 Ga mudstone, but the sources of these organic
284   molecules was not constrained [43,47]. Observation of dichlorobenzene and trichloromethylpropane in the
285   CB sample at Yellowknife Bay could have been produced by chemical reactions between organic
286   molecules and oxychlorines occurring in the SAM ovens. These chlorinated hydrocarbons could have
287   been derived from organic carbon, either from an endogenous martian source and/or from meteoric infall
288   [44,53]. Though organic carbon has been detected by SAM in numerous sedimentary deposits at Gale Crater,
289   the source(s) of the organic molecules are not yet fully understood. Recent work has shown that organic
290   salts such as Ca/ Mg oxalates and/or Ca/Mg acetates may be present in abundances of 1-2 wt. % in
291   modern eolian sediments (Rocknest sample) as well as in ancient sedimentary rocks at Gale Crater (JK
292   and CB samples) [54]. The accumulation of organic salts in eolian deposits suggests they may be a
293   component of regional or global dust on Mars [54].
294

1.5 Thermal analysis of organic carbon in modern soils and paleosols

296   Thermal analysis techniques similar to SAM-EGA have been employed for understanding the
297   nature and stability of organic matter in modern terrestrial soils, though at present there are only limited
298   studies of paleosols [30,39]. Past work has shown the thermal decomposition of organic carbon (C) is related
299   to organic carbon composition and particle size in both modern soils [55,56] and paleosols [57]. In modern soils
300   there is an inverse relationship between particle size and proportion of plant biopolymer-derived organic
301   carbon (carbohydrates, lignin) and C from microbial biomass and/or metabolites (protein, aliphatic C) [55].
302   Larger particle sizes are predominantly associated with labile remains of plant biopolymers, while the
303   clay-size fraction hosts highly recalcitrant (stable) C compounds which include microbial biomarkers of
304   n-C_{14} alkanoic acid [58]. Organic C associated with the clay-size fraction thermally decomposes at higher
305   temperatures (~ 400 - 450° C) compared to C associated with larger size fractions (~150° - 350° C) [57,59].
306   Thus, the thermal stability of organic carbon associated with clay minerals and/ or persisting as
307   microaggregates reflects increased resistance to oxidation [56] which is one factor among many contributing
308   to stabilization over geological time scales[60].
309

1.6 Preservation of organic matter in Archean paleosols

311

312   Life on Earth has a long history with soil, and some of the oldest biosignatures of life on land are
313   found in paleosols [61–63]. Transmission electron microscopy of the clay size fraction of an Archean (2.6
314   Ga) paleosol from South Africa showed organic carbon in association with surfaces and interlayer spaces
315   of clay minerals, possibly derived from cyanobacterial mats [17]. An Archean (~2.8 Ga) paleosol from
316   Western Australia contained filamentous, carbon-rich microstructures with regular banding and consistent
317   shape and size [18]. These structures, which contain up to 0.1 wt. % carbon, have been interpreted as
318   putative microfossils of methanogenic microbial mats living on the soil surface[18]. In both Archean
319   paleosol examples, organic carbon was most concentrated in near-surface horizons. Near-surface layers of
320   other Archean paleosols contain additional biosignatures such as isotopically light carbon [64] and sulfur [65].
321   Early Archean (3.7 Ga) metasedimentary deposits from the Isua supercrustal belt in Greenland which
322   have been considered putative paleosols [64] have $\delta^{13}C_{organic}$ of -24.2 to -27.4 ‰ and show mineralogical

323   evidence of subaerial acid-sulfate weathering, including abundant crystals of ripidolite interpreted to be
324   pseudomorphs of the sulfate mineral kieserite. These appear to be grouped into a gypsic (By) horizon
325   within a matrix of bertherine schist. Bertherine, a phyllosilicate in the serpentine group, is thought to have
326   formed from metamorphism of a trioctahedral phyllosilicate like saponite [64], thus implying that early
327   Archean Earth surface weathering may have been comparable to late Noachian surface weathering on
328   Mars. The putative Greenland paleosol has been tortured by metamorphism to amphibolite facies and thus
329   any biogenic source for the isotopic fractionation and/or discrimination should be interpreted with
330   caution. In any case, terrestrial paleosols provide compelling evidence of life's ancient relationship with
331   surface environments on Earth, which appears to extend well back into the Archean [17,18,61,66,67].
332   Though there appear to be similarities between the modes of weathering on the Early Earth and
333   Mars (e.g., anoxic acid sulfate weathering), the use of Archean paleosols as Mars analogs is complicated
334   by severe diagenetic overprinting that often obscures the original mineralogy and organic content of these
335   ancient land surfaces. Younger, less altered paleosols are more suitable candidates for comparisons with
336   putative paleosols on Mars, yet, as discussed below, these are also imperfect Mars analogs.
337
338

339   **1.7 Limitations of Cenozoic Mars-analog paleosols**
340   The Eocene-Oligocene (42-28 Ma) eastern Oregon paleosols are an incomplete Mars analog due
341   to several fundamental differences. First, the source of organic carbon within the paleosols is primarily
342   from microbial and/or plant biomass and represents a complex consortium of life above and within the
343   soil profile. Therefore, the organic carbon component of these paleosols and the resulting preservation
344   and degradation mechanisms may not be the same on Mars, but it is possible that putative paleosols at
345   Mawrth Vallis have mineralogy analogous to terrestrial paleosols and thus have a similar mineralogical
346   control on the fate of organic carbon. Nevertheless, the purpose of this study was not to determine the
347   "inputs" of organic carbon in paleosols, but rather to observe the "outcomes" of life on land, e.g., if and
348   how organic carbon is preserved across ancient surface environments.
349   A principal concern of this work was the assumption that all organic carbon in any lithified
350   paleosol sample was endogenous (e.g., deposited during soil formation) and has subsequently been
351   preserved for ~30 million years. This assumes no contribution from modern plants or microbes or
352   diagenetic alterations which add exogenous organic carbon. For example, modern soils developing atop
353   paleosol outcrops could have delivered exogenous organics to the underlying paleosols.
354   Another concern is the suite of common diagenetic alterations which alter paleosols, including
355   zeolitization, illitization and burial decomposition of organic carbon which appear to have affected
356   paleosols examined here to some degree (see Results). However, these are all are assumed to remove
357   endogenous organic carbon [1], not deliver it. We tested the hypothesis that organic carbon is endogenous
358   to paleosols by radiocarbon dating bulk samples (see Methods).
359   Large differences in age (Oligocene, [33 Ma] versus Noachian [4.1-3.7 Ga]) also have
360   implications for diagenesis. John Day paleosols have experienced a range of minor to moderate diagenetic
361   alteration including illitization of smectite, zeolitization and celadonization all resulting from alteration to
362   clinoptilolite facies [9,23], but it is currently unclear if similar diagenetic alteration has affected potential
363   paleosol sequences on Mars. There are also differences in the oxidation state of the atmosphere during
364   subaerial weathering. The Oregon paleosols formed under a thoroughly oxidizing atmosphere but at
365   present the oxidation state of an early Mars atmosphere is not well constrained [68], However, leaching of
366   Fe^{2+} in putative martian paleosols at Mawrth Vallis has been inferred from spectral weathering indices

367   and is consistent with an anoxic, reducing atmosphere during the Noachian [6]. Lastly, there are most likely
368   differences in the pH of fluids participating in hydrolytic weathering of volcaniclastic sediments. John
369   Day paleosols are thought to have formed by pedogenic weathering with circumneutral-pH fluids, but
370   subaerial alteration on Mars could have preceded with acidic, H_2SO_4 and HCl-rich surface waters as a
371   result of volcanic outgassing of H_2 and SO_2 [2,6]. Despite these significant differences, the paleosol
372   sequence from eastern Oregon offers a natural example to determine if organic carbon can be detected
373   with thermal and evolved gas analysis techniques similar to SAM-EGA.
374

375   **2. Methods**

376   **2.1 Sample collection**

377   The paleosols examined in this study were collected from the Painted Hills Unit of the John Day
378   Fossil Beds National Monument in eastern Oregon, USA. A previous study **(Broz et al., 2021, in review)**
379   determined the mineralogy and diagenetic alteration of the same set of samples examined in the present
380   study. Samples from three individual paleosols in vertical succession were collected approximately 7 km
381   SW of the entrance to the Painted Hills unit of the John Day Formation (44.631105, -120.213107), in the
382   Middle Big Basin Member of the John Day Formation, approximately 6 m above the local Eocene-
383   Oligocene boundary **(Figure 2).** Samples were chosen from this location because they were previously
384   examined for mineralogy and diagenesis, and because $^{40}Ar/^{39}Ar$ dating of volcanic tuffs at this
385   stratigraphic level in the section allow for a constrained age of 33.0 +/- 0.10 to 32.7 +/- 0.03 Ma (Biotite
386   Tuff and Overlook Tuff, respectively) [22].

387   To minimize contamination from modern organic carbon during sampling, all loose surface soil
388   and saprolite was removed until the lithified, brick-like unweathered paleosol surface was exposed.
389   Below the saprolite of the thin (~30 cm) modern soil, all three paleosols were lithified claystone. Sample
390   collection began by trenching with a rock hammer to a 50 cm depth into (perpendicular to) the lithified
391   paleosol sequence. Next, a set of samples were gathered down a vertical transect at approximately 10 cm
392   intervals, similar to sampling the horizons of a modern soil, but with rock hammer. Large (~1 kg) lithified
393   blocks of claystone were broken out of the outcrop and placed into aluminum foil (ashed at 550° C before
394   use) to ensure subsampling for thermal analysis had sufficient volume to expose fresh sample surface
395   (e.g., no weathered surfaces were selected for analysis). For thermal analysis and radiocarbon dating,
396   small (5-8 g) subsamples were acquired from the inside of bulk lithified samples with steel chisels that
397   were previously ashed at 550° C to remove organic contaminants. These subsamples were then ground to
398   < 0.02 mm using an agate mortar and pestle (ashed at 550° C before use) and stored in glass vials (all
399   ashed at 550° C) prior to thermal analysis and radiocarbon dating.

400   No vegetation was present within ~30 m of the sampled paleosol sequence **(Figure 2),** likely
401   because the "popcorn" weathering of the smectite-rich modern soil appears to inhibit plant germination
402   and growth**.** The Munsell color and qualitative calcareousness of samples were described during
403   collection **(Figure 3).** The three paleosols sampled were a red Alfisol ("Luca" pedotype from [23]), a tan
404   Entisol ("Kskus" pedotype), and a brown Inceptisol ("Ticam" pedotype **(Figure 3, Table S1**).
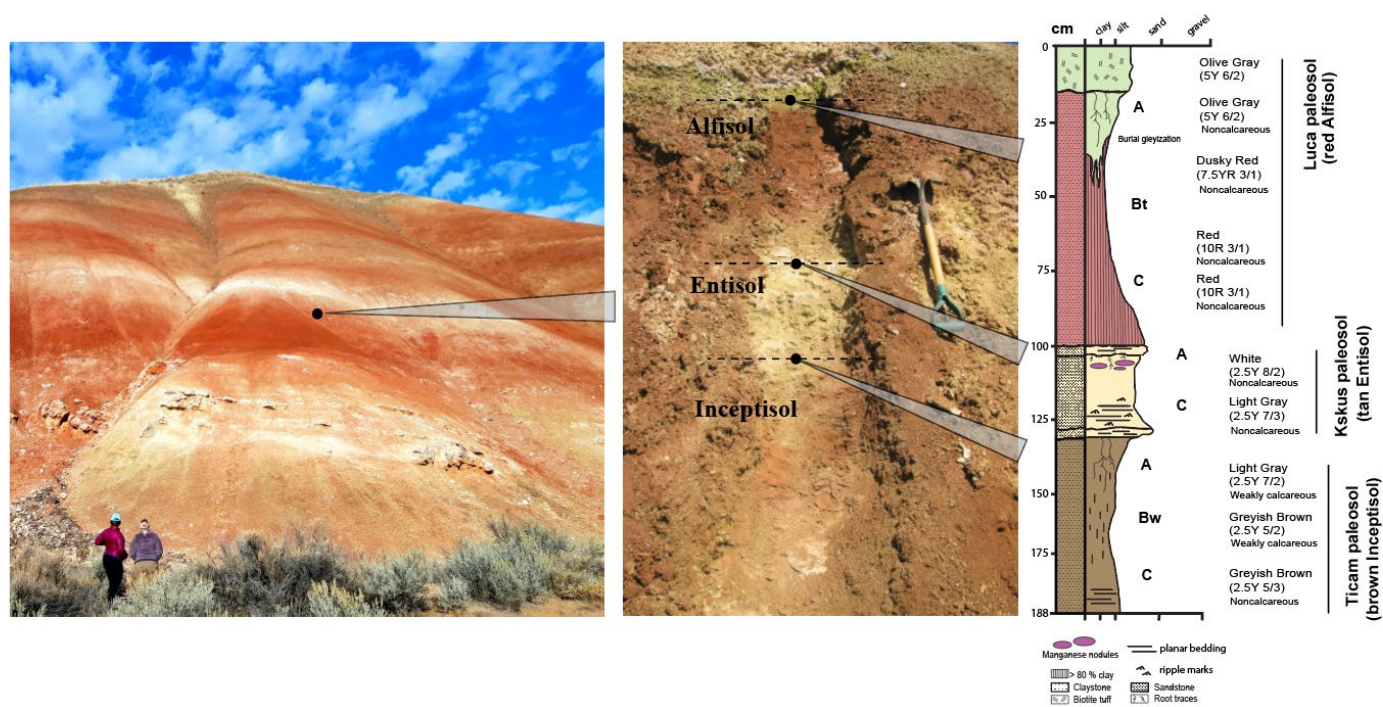
406 **Figure 3. Morphology of three successive paleosols** from the early Oligocene (33 Ma) middle Big Basin Member
407 of the John Day Formation in eastern Oregon, USA showing lithology, grain size, horizon designations, and Munsell
408 color. The upper paleosol (red with drab green top) is a moderately weathered red Alfisol (Hapludalf in USDA
409 Taxonomy); stratigraphically below is a minimally weathered and weakly developed Entisol (Fluvent; tan color); the
410 lowest soil (brown color) is an Inceptisol (Andic Eutrochrept, brown color)

2.2 Radiocarbon dating of organic carbon in paleosols

412   The purpose of radiocarbon (^{14}C) dating was to constrain the age of organic carbon in paleosol
413 samples. Specifically, radiocarbon dating was used to determine if the organic carbon fraction of
414 paleosols was entirely endogenous (deposited during soil formation) and had been preserved for millions
415 of years, or if there had been additions of exogenous organic carbon to paleosols in the last ~45,000 years
416 (the method-level detection limit for radiocarbon dating techniques). A radiocarbon age of organic carbon
417 was obtained from four samples, two from the surface and near-surface horizons (A and Bt horizons) of
418 the stratigraphically highest soil (Alfisol) and two from the surface and near-surface horizons of the
419 stratigraphically lowest profile (Inceptisol). All samples for radiocarbon dating were acid-washed to
420 remove inorganic carbonates before radiocarbon dating. For acid washing, ground paleosol samples (~5
421 g) were treated with approximately 20 mL of 0.1 M HCl at room temperature, then washed three times
422 with ~30 ml of deionized water and dried at 60° C for 24 hr. Radiocarbon dating of acid-washed paleosol
423 samples was performed at the W.M. Keck Carbon Cycle Accelerator Mass Spectrometer at the University
424 of Irvine. The accuracy and precision (1 σ) of this analysis on modern carbon (Δ^{14}C >0%) was better than
425 9‰. Laboratory blanks yielded a Δ^{14}C value of -996.2 ‰.

2.6 Thermal and evolved gas analysis of paleosol samples

427   The purpose of this work was to use SAM-EGA-like conditions to characterize bulk gas evolution
428 and to measure abundance of organic and inorganic carbon in Mars-analog paleosol samples. A Setaram
429 Labsys Evo differential scanning calorimeter (DSC) / thermal gravimeter (TG) connected to a Pfeiffer
430 Omnistar QMS was configured to operate similarly to the SAM evolved gas analyzer. The SAM
431 instrument does not have TG/DSC capabilities, but these components permit a better understanding of
432 phase transitions and chemical reactions in laboratory experiments. Approximately 50 mg ± 3 mg of
433 ground paleosol sample (previously stored in glass vials ashed at 500° C to minimize organic
434 contamination) were placed in an Al_2O_3 sample crucible which was ashed at 500° C to remove organic
435 contaminants before use. The sample crucible and an identical empty reference crucible were placed in
436 the furnace and then the system was purged twice with helium gas and then set to a pressure of 30 mbar.
437 Helium was chosen as a carrier gas because it is inert and because it used as a carrier gas in the SAM
438 instrument. The crucibles were heated from approximately 35 °C to 1000 °C at a heating rate of 35°C/min
439 and at a flow rate of 10 sccm. Volatiles ranging from mass/charge (m/z) 1 - 100 were measured. All
440 analyses were performed in duplicate.

441   Total organic carbon (TOC) content was determined using a Netzsch TG/DSC coupled to a
442 Pfeiffer QMS. Typical TOC determinations via elemental analysis involve an acid pretreatment step to
443 remove carbonates, but acid pretreatments have been shown to alter the original organic carbon content of
444 samples[69]. Paleosol samples were not acid-pretreated for thermal and evolved gas analyses because some
445 organic carbon can be oxidized during acid-washing [69]. An Al_2O_3 sample crucible and an identical
446 reference crucible were placed in the furnace. The instrument was purged twice with ultra-high purity O_2
447 and set to a pressure of 1000 mbar prior to sample analyses to remove any contamination in the system.
448 Oxygen was chosen as a carrier gas because it encourages complete combustion of all organic and
449 inorganic carbon in samples. The crucibles containing samples were heated from approximately 35 °C to
450 1000 °C at a heating rate of 35°C/min and at a flow rate of 19 ml O_2/min. A series of three blanks were
451 analyzed before and after each group (n=10) of samples. A calibration curve for CO_2 was created by
452 analyzing a calcite standard (Iceland sparry calcite 40 ųM) at eight sample masses ranging from 0.01 – 4
453 mg (Table S1). This calibration curve was used to calculate the amount of CO_2 evolved from each
454 sample, and these values were used to calculate total organic carbon. In the present study, carbon was
455 considered organic between 150-550° C and inorganic from ~700-900° C. Organic C was quantified by
456 deconvolving CO_2 peaks if a carbonate-C peak was present. This was done by determining the relative
457 percentage of peak area from inorganic carbon-evolved CO_2 (~700-900° C) then subtracting this value
458 from total carbon-evolved CO_2 peak area to solve for total organic carbon. All evolved gas plots were
459 background-corrected to account for possible atmospheric contamination.

460   Thermal techniques including TG-DSC-EGA allow for quantitative estimates of organic and
461 inorganic carbon. Inorganic carbon decomposition or combustion evolves CO_2 at high temperatures
462 (~700-900° C) and thus can be distinguished from low temperature (~150-550° C) CO_2 evolutions from
463 the decomposition of organic carbon [46,59]. Iron carbonates such as siderite can decompose in the 450° C
464 range, but previous mineralogical investigation of these samples found no evidence of iron carbonates
465 **(Broz et al 2021, in review).** Thus, the large temperature gap and differences in the thermodynamics of
466 organic and inorganic C decomposition make this method ideal for examining soil and paleosol organic
467 matter without the need for acid pretreatment (e.g., acid fumigation) for carbonate removal.

468 **3. Results/Discussion**

469   **3.1 Radiocarbon dating of paleosol organic carbon**
470
471   Radiocarbon dating of four samples from two different paleosol profiles showed ages between 6265 ±
472   25 years BP and 14560 ±170 years BP (Table 1). These samples all showed a distinct signature of
473   exogenous organic carbon because the samples were not radiocarbon dead (^{14}C-free).
474

Table 1. Total organic carbon (TOC), total inorganic carbon (TIC) and radiocarbon dating of paleosols exam

Paleosol	Pedotype [‡]	Horizon [φ]	Depth in profile (cm)	Total C (wt. %)	TOC (wt. %)[†]	±σ TOC [§]	TIC (wt. %)	Expected Age	Δ^{14}C[‡]	±Δ^{14}C
Alfisol	Luca	A	4	0.073	0.031	0.0062	0.042	~33 Ma	-543.07	3.85
Alfisol	Luca	A	14	0.094	0.026	0.0097	0.068			
Alfisol	Luca	Bt$_1$	46	0.021	0.018	0.0016	0.003	~33 Ma	-838.12	3.37
Alfisol	Luca	Bt$_2$	63	0.067	ND [ʊ]	-	0.067			
Alfisol	Luca	C	88	0.033	0.002	0.007	0.031			
Entisol	Kskus	A	100	0.046	0.021	0.0068	0.024			
Entisol	Kskus	C	120	0.036	0.013	0.0037	0.024			
Inceptisol	Ticam	A	125	0.024	0.018	0.007	0.006	~33 Ma	-567.1	1.83
Inceptisol	Ticam	Bw$_1$	131	0.027	0.008	0.0013	0.019			
Inceptisol	Ticam	Bw$_2$	160	0.020	0.011	0.0023	0.010	~33 Ma	-545.4	1.33
Inceptisol	Ticam	C	175	0.026	0.001	0.0013	0.026			

† Determined by thermal analysis (TG-DSC-EGA) without acid pre-treatment of samples; average of two
duplicates. To encourage complete combustion of organic phases in samples, oxygen was used as a carrier gas
for determination of total C, TIC and TOC.
‡ Pedotypes (soil orders) are from Retallack et al. 2000
φ Horizons follow USDA Soil Survey Staff (2014) major horizon designations
ʊ ND = No detection; below limit of quantification
§ Standard error for TOC determination from duplicate analysis
‡ Radiocarbon concentrations are given as fractions of the modern standard (fM), Δ^{14}C, and conventional
radiocarbon age.

475
476
477   The occurrence of Holocene-age organic matter in paleosol samples was consistent with
478 diagenetic inputs of organic C. There are several possibilities to explain the accumulation of ^{14}C in the
479 organic fraction of samples. First, a diagenetic event that occurred between ~6 and ~14 Ka BP could have
480 delivered exogenous organics into the underlying paleosols, perhaps during exhumation to the surface and
481 /or leaching of organic acids from surface biota during that time. Cosmogenic exposure dating such as
482 [10]Be surface exposure dating would provide important evidence to constrain the exhumation history of the
483 paleosols examined here [70,71]. However, there was no sedimentological evidence of exhumation and re-
484 burial of any of the three paleosols at the field site, so other possibilities to explain the radiocarbon dates
485 were explored.
486   Another possible source of exogenous organic carbon was from precipitation-driven leaching of
487 dissolved organic carbon from modern biota living in the current weathering zone above the paleosol
488 outcrop. The fraction of modern carbon (fM) across four samples ranged from 0.469 ± 0.039 to 0.1633 ±
489 0.034 (Table 1) and was highest in the surface (A horizon, 14 cm) of the Alfisol and lowest in the
490 subsurface (Bt horizon, 46 cm), suggesting this paleosol contained a mixture of ancient and modern
491 organic carbon, the latter possibly delivered via precipitation-driven leaching. As such, it is possible that
492 small amounts of exogenous modern organic carbon from the weathered zone above paleosol outcrops

493   have mixed with larger amounts of ^{14}C-free organic carbon endogenous to paleosols. In this way, a

494   radiocarbon date of ~6-14 Ka BP could represent a mixing of recent/modern organic carbon and ~33 Ma

495   organic carbon. This hypothesis is supported by the erosion rate for the site, which was previously

496   determined to be 4.94 ± 0.05 mm/yr [72]. Using this erosion rate, the 20 cm-thick soils that formed on top of

497   the paleosols are only about 40 years old and could have leached modern organics into the underlying

498   paleosols during this time.

499   There was also a weak relationship between the radiocarbon age and the depth into the outcrop

500   where the sample was collected (Table 1). Younger radiocarbon dates were observed in shallower

501   samples taken closer to the modern weathering zone. However, a decrease in ^{14}C content with depth is

502   commonly observed in modern soils because subsurface horizons preferentially accumulate older,

503   refractory organic carbon primarily via sorption to surfaces of minerals and amorphous phases [73]. Across

504   four paleosol samples in this work, the radiocarbon age generally increases with depth, suggesting there

505   may be age-depth relationship for samples (Table 1), but this result should be interpreted with caution

506   because only four samples were dated in this work, and because age-depth trends are routinely observed

507   in modern soils [74]. In any case, there may be a sampling depth (i.e., > 1 meter) that significantly reduces

508   or eliminates exogenous carbon additions to paleosols. These results highlight challenges for studying the

509   organic fraction of paleosols while also demonstrating that radiocarbon dating can be a useful technique

510   for constraining organic matter preservation in ancient terrestrial surface environments.

511

512   **3.2 Thermal and Evolved Gas Analysis**

513   **3.2.1 CO_2 and CO evolutions**

514   When subject to thermal and evolved gas analysis, all samples evolved CO_2 at temperatures

515   ranging from ~150 – 800° C and had two distinctive CO_2 peaks (Figure 6). A broad low temperature

516   ~200-500° C peak was followed by a sharp high-temperature peak at ~650-750° C which was observed in

517   all samples. CO_2 evolved at 150-500° C is primarily from organic carbon decomposition [69,75] but also

518   possible are contributions are from CO_2 inclusions in minerals or amorphous phases, or from adsorbed

519   atmospheric CO_2 [46]. The organic C contributing to evolved CO_2 is most likely from simple organic

520   compounds (<350° C) or refractory macromolecular organic compounds (300-600° C) [43].

521   The endothermic thermal decomposition of Ca carbonate was a probable source of CO_2 release

522   from approximately 550 – 800° C [76,77]. High temperature (> 650° C) CO_2 evolutions generally exceeded

523   the low temperature (150-550° C) CO_2 evolutions in peak area across all samples, though both high

524   temperature and low temperature CO_2 evolutions were on the same order of magnitude. Total inorganic

525   carbon (TIC) values varied from 0.006 to 0.068 wt. % (Table 1) and the ratio of inorganic carbon to total

526   carbon ranged from 0.14 to 1, consistent with variable mixtures of Ca carbonate and organic carbon in

527   each sample. There are well-defined Ca carbonate endotherms in the heat flow data from the Entisol and

528   Inceptisol, but this trend was not so well-defined in the Alfisol (Figure 6) and there also appears to be

529   "doublet" high-temperature CO_2 peaks for the Entisol, suggesting a combination of Ca-carbonate and

530   perhaps dolomite or ankerite, though these phases were not previously observed in XRD diffractograms

531   (**Broz et al., 2021**, in review). DSC-EGA analysis of modern soils containing various amounts of calcite

532   have a similar sharp endothermic CO_2 peak release temperature at ~700° C which was attributed to the

533   thermal decomposition of Ca carbonate [69]. An additional ~900° C endotherm observed in all samples was

534   unrelated to carbonate decomposition and instead was attributed to thermal decomposition of sulfate

535   minerals such as jarosite, which was previously detected in trace amounts with x-ray diffraction (**Broz et

536   al., 2021**, in review). Interestingly, Ca-carbonate was not previously identified from x-ray diffraction

537   patterns, and thus it is likely that these samples contain inorganic carbonate below detection limit of XRD
538   (~1 wt. %), but not SAM-EGA (0.01 wt. %). This agrees with estimated abundances of TIC which were
539   below 1 wt. % (Table 1) and demonstrates the ability of SAM-EGA-like analyses to detect trace amounts
540   of inorganic carbon in complex pedogenic mineral matrices.
541   Other sources of high temperature CO_2 release could have result from the decarboxylation of
542   organic compounds in refractory or thermally mature organic matter which occur over a broad range of
543   temperatures (150 - 800° C). Previous investigation showed no coalification of organic matter or
544   development of secondary porosity in any paleosols from the Painted Hills, which were buried by an
545   estimated 1.5 - 2 km of overburden [9,23], suggesting paleosol samples here contain refractory but not
546   thermally mature organic compounds.
547
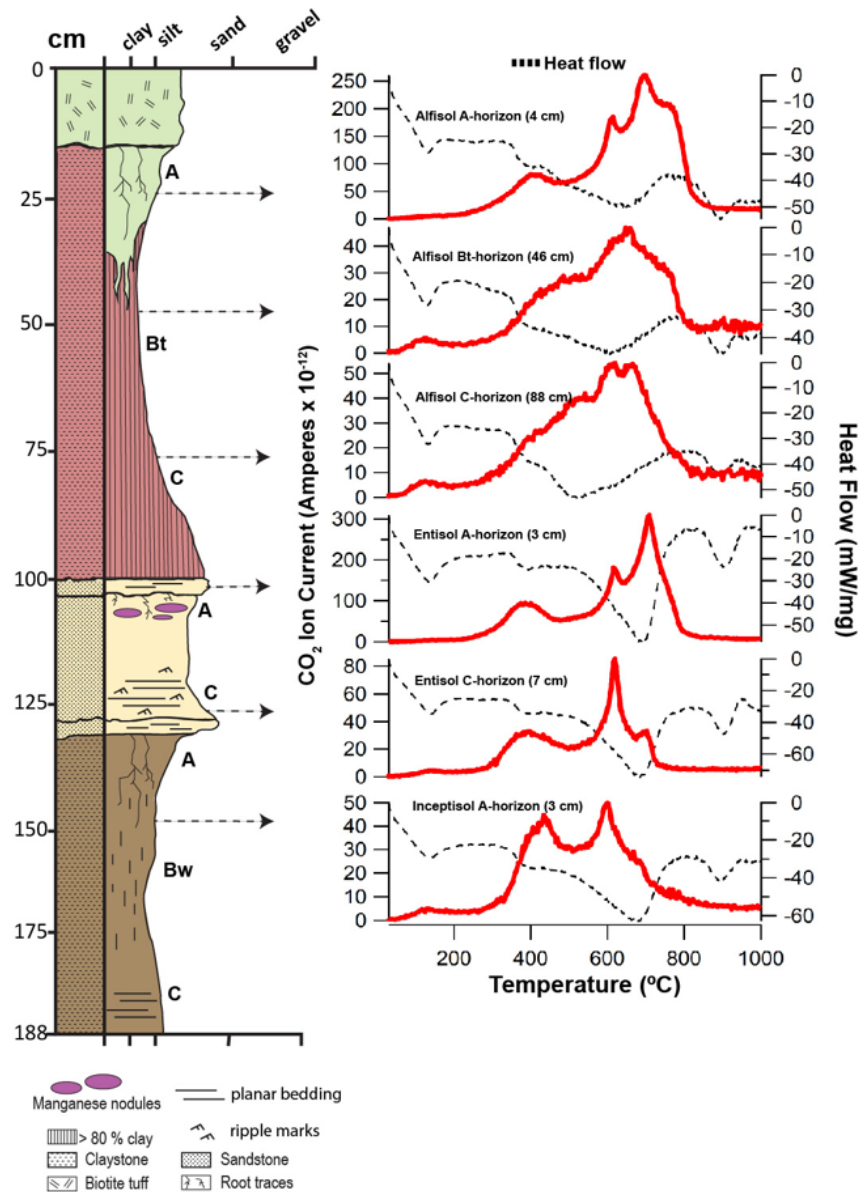
549   **Figure 6. Evolutions of CO_2 (red traces) and heat flow (dashed traces) from early Oligocene (33 Ma) smectite-**
550   **rich paleosols from the John Day Fossil Beds National Monument, Oregon.** Red trace is CO_2 (m/z 44) and

551   dashed trace is heat flow from differential scanning calorimetry (DSC). Helium was used as a carrier gas for all
552   analyses.
553
554   All samples evolved CO with a peak release temperature of ~400° C (Figure 7). The sample with
555   the highest total organic carbon detected (~0.03 wt. %, surface horizon of Alfisol) evolved a CO_2 release
556   peak at ~400 °C that co-occurred with the release of CO. This trend of coevolved CO and CO_2 at ~400° C
557   was observed across all paleosol samples. Evolution of CO was consistent with incomplete combustion of
558   organics and/ or the presence of oxygen-bearing organics [75]. The co-occurrence of CO and CO_2 was not
559   observed at high (~700 °C) temperatures (Figure 7) because the thermal decomposition of Ca carbonate
560   does not produce CO. Thus, evolved CO detections near 400° C were consistent with the decomposition
561   of organic compounds.
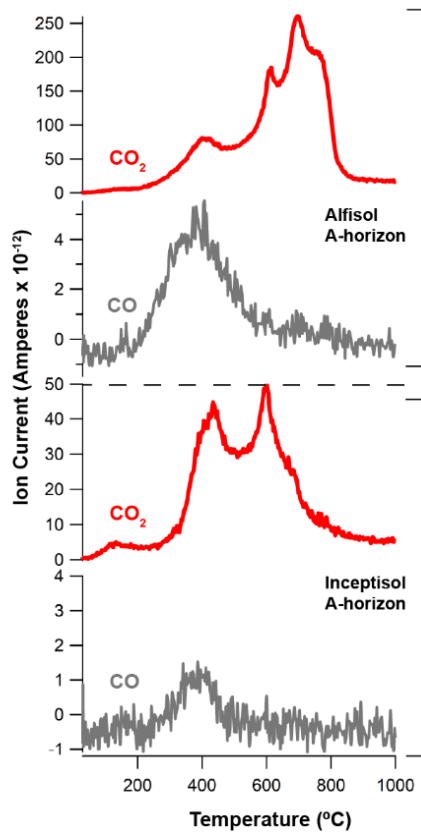
563
564   **Figure 7. CO_2 (red trace) and CO (m/z 28) (grey trace) evolutions from the surface horizons of smectite-rich**
565   **paleosols at the John Day Fossil Beds National Monument, Oregon. Top panel is** surface (4 cm) horizon of an
566   Alfisol; bottom panel is surface (3 cm) horizon of an Inceptisol
567
568
569
570   **3.2.2 NO evolutions**
571   Nitric oxide (NO; m/z 30) was detected in all paleosol samples (Figure 8) and was consistent with
572   the oxidation of nitrogen-bearing organics. In the sample with the greatest amount of organic carbon
573   (Alfisol A-horizon), evolutions of NO start at ~300° C and show peak release temperature of ~ 400° C
574   and a shoulder at ~ 600° C (Figure 8). Additionally, organic fragments observed in this sample included

575   CH_2 (m/z 14), CH_3 (m/z 15), and C_2H_2 (m/z 26) (Figure 9). Evolutions of NO were simultaneous with

576   evolutions of these organic fragments at ~400° C, suggesting the oxidation of a nitrogen-bearing organic

577   compound was a significant contributor to evolved NO [78].
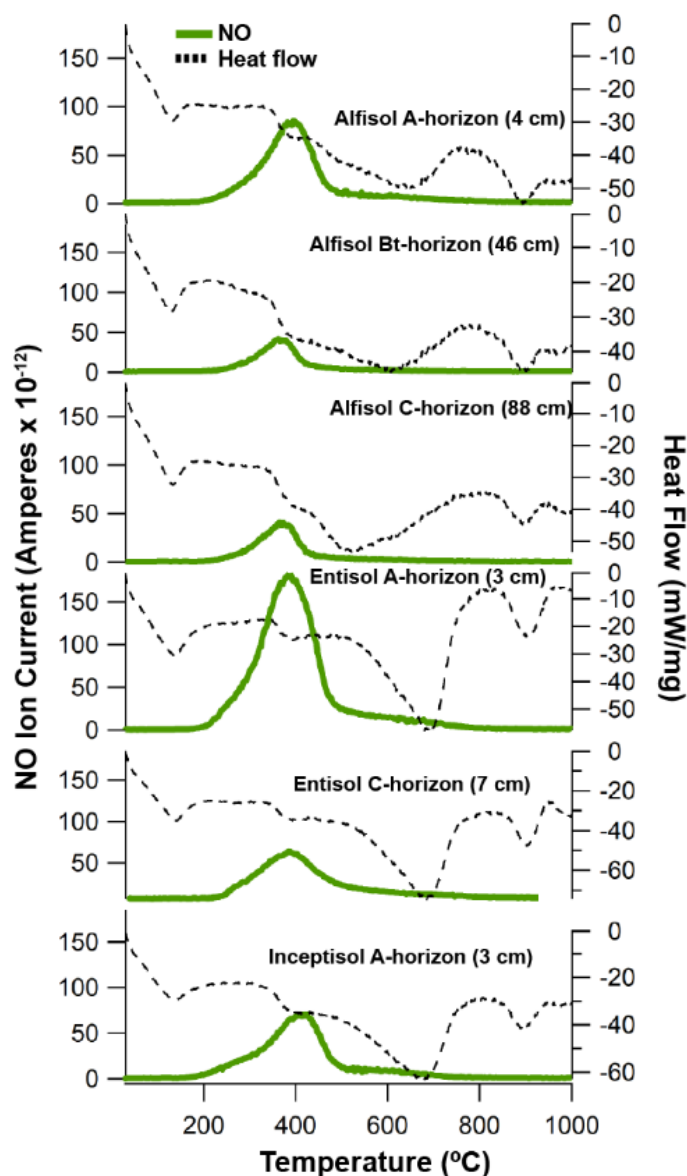
579   **Figure 8. Evolutions of nitric oxide (NO) from smectite-rich paleosols at the John Day Fossil Beds National**

580   **Monument, Oregon.** Green trace is NO (m/z 30) and dashed trace is heat flow from differential scanning

581   calorimetry (DSC).

582

583

584   The thermal decomposition of nitrates can also release NO, though at elevated temperatures (>

585   500° C) relative to nitrogenated organics [78], and therefore the release peak temperate of NO release can

586   constrain the source of NO. For example Alkali (Na, K) and alkaline earth (Mg, Ca) metal nitrates

587   decompose to NO at temperatures > 560° C [78]. In laboratory experiments under SAM-like conditions,

588     $Fe(NO_3)_3$ begins to decompose to NO at < 200° C and exhibits two distinct releases of NO at ~300 and

589 ~450° C, which has been attributed to dehydration and hydrolysis of $Fe(NO_3)_3$, respectively [78]. Instead,
590 NO release in paleosol samples began at ~250° C and exhibited a single peak at ~400° C across all
591 samples **(Figure 8)**, unlike the dual high-temperature NO peaks from decomposition of $Fe(NO_3)_3$. The
592 simultaneous evolution of NO, CO_2, and organic fragments in paleosol samples analyzed here (Figure 9)
593 are an additional line of evidence suggesting NO releases could have resulted from oxidation and/or
594 decarboxylation of nitrogen-bearing organic compounds.

595
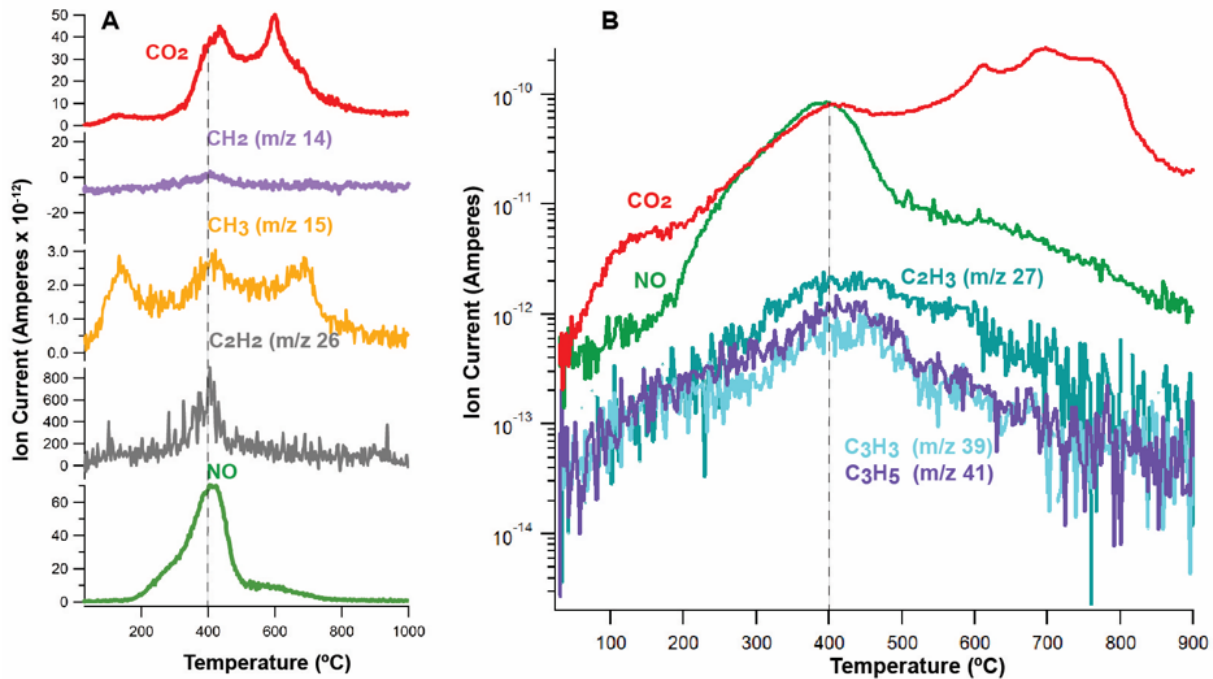
597 **Figure 9. Simultaneous evolutions of CO_2, NO (m/z 30) and organic fragments in paleosol surface horizons.**
598 **(A)** Evolutions of CO_2, NO (m/z 30), and organic fragments (m/z 14, 15, 26) from the surface horizon of the
599 Inceptisol (3 cm). **(B)** Semi-log scale plot of CO_2, NO and additional organic fragments (m/z 27, 39, 41) from the
600 surface horizon (4 cm) of the Alfisol.

601

602 One possible source of nitrogen-bearing organic carbon compounds is pyrogenic carbon (char) in
603 paleosol samples that formed as a result of wildfires across the original soil landscape [79]. Nitrogen-
604 bearing organic compounds such as nitriles, pyridine and pyrrole-derive compounds have been observed
605 with pyrolysis GC/MS in modern fire-affected soils [80]. These modern soils were also observed to have a
606 broad ~400° C peak release temperature of NO (m/z 30) during TG-DSC-EGA, suggesting that pyrogenic
607 carbon may be the source of low-temperature NO release in soils. However, the fire history of paleosols
608 in the present study has not yet been investigated. Although it is impossible to determine the original
609 inputs of nitrogen-bearing organics in paleosols, nitrogen may have been incorporated into increasingly
610 stable organic matter as a consequence of forest fires, and may persist in paleosols today as char. Previous
611 authors have reported the occurrence of preserved char in paleosols of late Permian[81] and late Jurassic
612 age[14] paleosols, respectively, so it is plausible that nitrogen-bearing char may be responsible for the
613 overlapping ~400° C NO and CO_2 peaks observed here.

614

615 **3.3 Possible mechanisms of organic carbon preservation in paleosols**

616   We observed evolutions of volatile gases from clay-rich paleosols that may have resulted from
617 the preservation of organic carbon over geological time scales. The fragmentation of organic molecules
618 during pyrolysis EGA provides limited constraints on the types of molecules present, but it can help
619 determine if there are any associations between minerals and organic molecules. These associations can
620 include physical occlusion, chemisorption and/or adsorption to mineral surfaces, or intercalation in clay
621 minerals [82–85]. A strong correlation between the peak release temperature of organic fragments and the
622 release of H_2O or other volatiles would suggest that organic matter could have been associated with
623 minerals.
624   One line of evidence that organic molecules may have persisted in association with clay minerals
625 is co-occurring evolutions of organic fragments, CO_2, and water releases from clay dehydroxylation. Al-
626 smectite in the surface horizon of the Alfisol began dehydroxylating at ~400° C (broad H_2O peak) which
627 co-occurred with evolutions of CO_2 and organic fragments (Figure 10). This sample had the highest TOC
628 (~0.03 wt. %, Table 1), a radiocarbon date of ~6300 years BP and a phyllosilicate content of ~85 wt. **%**
629 (Table S1**) (Broz et al., 2021).** The high clay mineral content could be related to the abundance of organic
630 carbon in this sample. However, additional investigations such as microscale imaging (e.g., transmission
631 electron microscopy) and methods to characterize the bonding environments between minerals and
632 organics in paleosols are needed to support this interpretation.
633
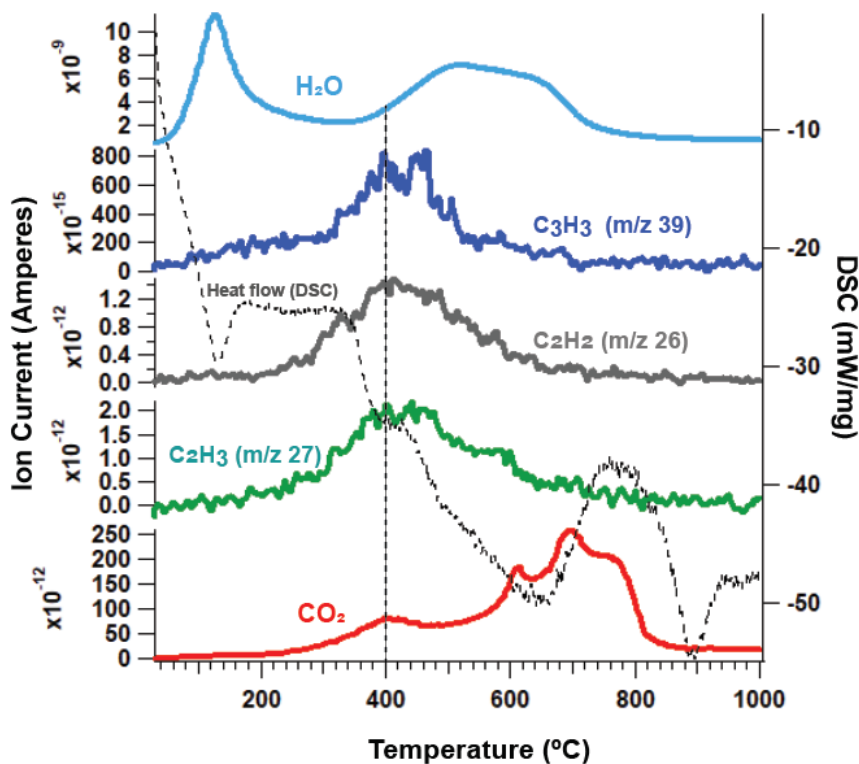
635 **Figure 10. Evolutions of CO_2, organic fragments, and H_2O from the surface horizon of the Alfisol (4 cm).** Co-
636 occurring releases of CO_2 and organic fragments at the onset of Al-smectite dehydroxylation (H_2O release at ~400°
637 C, vertical dotted line) suggest organic molecules may have been associated with clay minerals. Dashed trace is heat
638 flow from differential scanning calorimetry (DSC).
639

640   It is important to note that there are many competing factors that control the preservation and
641 degradation of organic carbon in terrestrial environments. Minerals themselves may facilitate oxidation of
642 organic carbon compounds [84], as is the case with certain Mn-bearing minerals [86]. Possible mechanisms of

643   organic carbon preservation in paleosols examined here include the formation of organo-mineral

644   complexes and/or the formation of microaggregates that may increase the biochemical stability of organic

645   molecules, as observed in modern soils [59] and Quaternary paleosols [57]. Paleosols examined here

646   contained between ~70-90 wt. % smectite, primarily as mixtures of montmorillonite and nontronite

647   (Table S2). Smectite clay minerals in particular preserve organic molecules due to their high specific

648   surface area, negatively charged interlayers, and cations which inhibit water flow, thus making them

649   favorable locations for the preservation of organic carbon over millions or possibly billions of years

650   [39,44,60].

651

652   Interactions with sulfur can also aid in the preservation of organic molecules in soils and

653   sediments over geological time scales [14,43,85,87]. The incorporation of organic C into the crystal lattice of

654   sulfate minerals can increase thermodynamic stability and therefore increase the temperature of organic

655   carbon decomposition during EGA[85]. Minor detections of jarosite and gypsum in XRD patterns (< 5 wt.

656   %) observed in all paleosol samples, and these minerals could have also contributed to the preservation of

657   organics. Minor SO_2 evolutions at 800° C across all samples (Figure S2) were consistent with the

658   decomposition of sulfate minerals and a single sample (Entisol 7 cm) had a low-temperature SO_2 peak

659   that co-occurred with the CO_2 release at ~400° C. Trace amounts of Mg sulfates in the Alfisol could

660   account for minor SO_2 releases > 700° C including the ~790° C SO_2 peaks [85,88]. At higher temperatures,

661   all soils showed a major release of SO_2 beginning at 900° C which co-occurred with an endotherm, both

662   of which are consistent with the thermal decomposition of crystalline sulfates [46,85]. Since the samples were

663   only heated to ~1000° C for this work, the maximum peak height of this release cannot be ascertained.

664   However, peak SO_2 release temperatures generally did not co-occur with low-temperature CO_2 evolutions

665   across the rest of the samples (Figure S2), so it is unlikely that sulfate minerals played a significant role in

666   organic preservation in samples examined here.

667

668
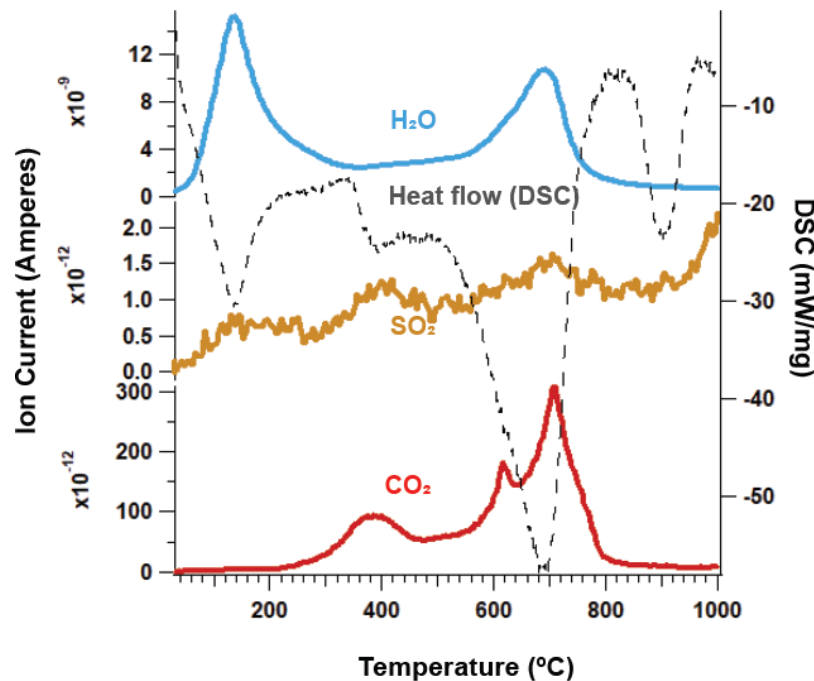
670 **Figure 11. Evolutions of H_2O (blue trace), SO_2 (yellow trace), CO_2 (red trace), and heat flow (dashed trace)**
671 **from the surface horizon of the Entisol (3 cm).** DSC – differential scanning calorimetry (heat flow), H_2O – m/z
672 18, SO_2 – m/z 64, CO_2 – m/z 44.
673

674 **3.4 Enrichment of organic carbon in surface layers of paleosols**
675   The near-surface horizons of all paleosols examined here had greater amounts of total organic
676 carbon (TOC) relative to deeper horizons (Figure 12, Table 1). The highest amounts of CO_2 released from
677 decomposition of organic carbon (150-500° C) were in the near surface (A) horizons of all three paleosol
678 types while subsurface layers of paleosols generally had lower quantities of evolved CO_2 from organic
679 carbon (Figure 6, Table 1). The A horizon of the Alfisol had TOC of 0.031 ± 0.006 wt. % and
680 progressively decreased to 0.002 ± 0.007 wt. % in the C horizon.
681   Samples from the A-horizon of the Alfisol had been affected by burial gleization. Burial
682 gleization is an early diagenetic process in paleosols which involves the reduction of Fe^{3+} to Fe^{2+} by
683 anaerobic microbes as a result of rapid burial [1,89]. This is also thought to promote anaerobic decay of
684 organic matter [1], even in soils that originally formed under oxidizing conditions before burial. Typical
685 burial gleization is closed system alteration, without depletion of total iron, and is usually limited to the
686 surface horizons where organic matter is most concentrated. The surface horizon of the Alfisol examined
687 in this work showed classic evidence of burial gleization with drab-colored mottles and tubular features
688 predominantly in the A-horizon with minor radiation downward into the subsurface (Bt) horizon (Figure
689 12). Rapid emplacement of a biotite-bearing tuff on the paleosurface of the Alfisol may have led to
690 gleization. Similar trends of near-surface TOC enrichment were noted in the Entisol and Alfisol (Table 1),
691 but these samples lacked chemical and morphological evidence of burial gleization **(Broz et al., 2021, in**
692 **review).** Previous work on terrestrial paleosols has shown positive and significant correlations between
693 Fe^{2+} and TOC [13]. This supports the interpretation that burial gleization, which increases Fe^{2+} in bulk
694 samples, may have been associated with the preservation of organic carbon in the surface horizon of the
695 Alfisol.

696
697
698
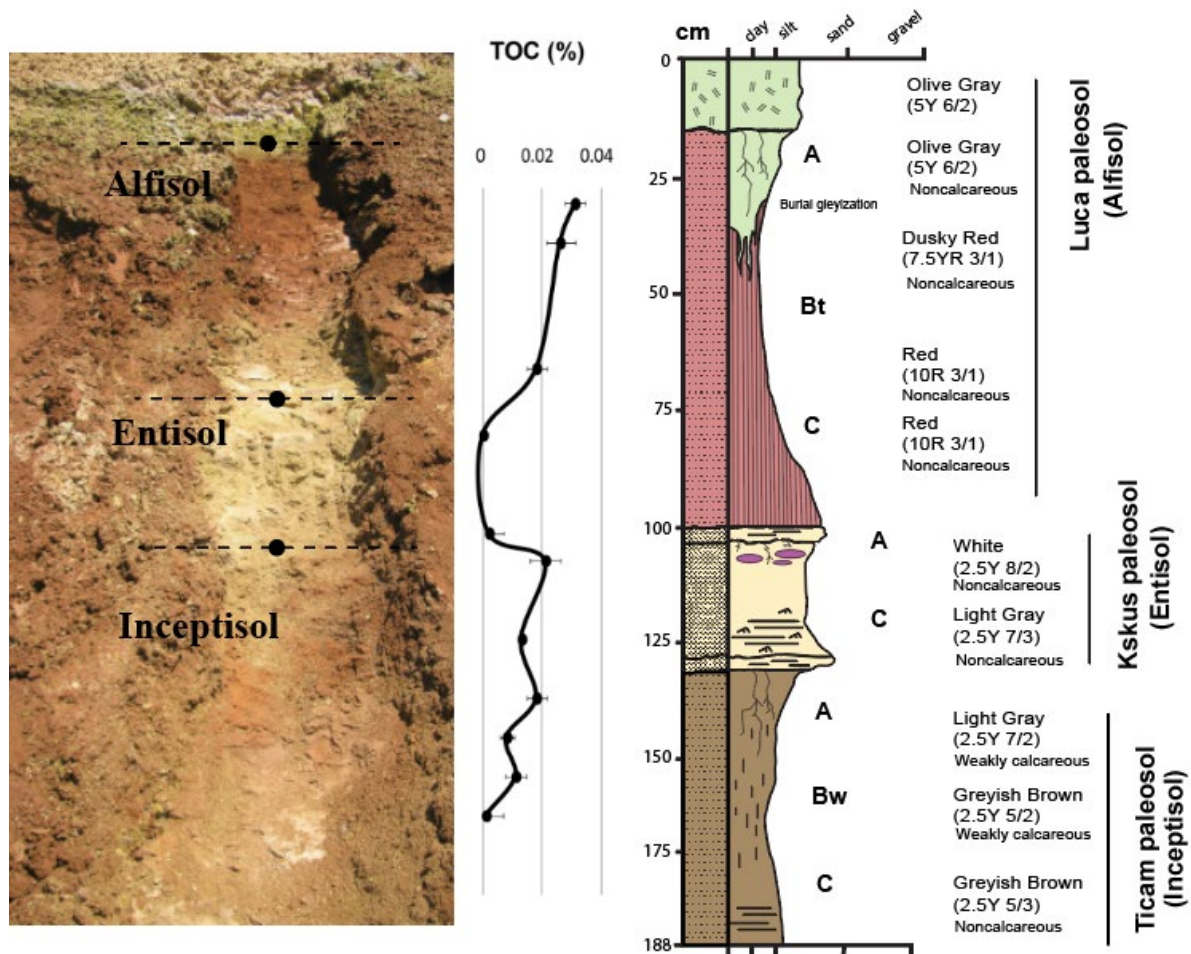
Figure 12. Trends of organic carbon enrichment in the near-surface horizons of three paleosols from the early Oligocene (33 Ma) middle Big Basin Member of the John Day Formation in eastern Oregon, USA**.** The surface (A) horizons of all three profiles had significantly ($P > 0.05$) higher total organic carbon (TOC) content relative to subsurface horizons (Bt, Bw and C horizons, respectively). Average TOC content of samples (n=2) was determined by thermal and evolved gas analysis (oxygen as a carrier gas).

Organic carbon from organisms living in surface horizons of soils may have been preserved upon rapid burial of the paleosurface, and therefore the trend of surface enrichment may represent the preservation of endogenous organic carbon. Alternatively, diagenetic additions of carbon may have accumulated in near-surface layers of each profile. Major losses of endogenous organic carbon from early diagenetic burial decomposition of organic matter are common in paleosols that originally formed under oxidizing conditions such as those examined here [1]. Despite diagenetic additions and losses of organic carbon, the trend of surface enrichment of organic carbon remains apparent, even in soils that formed under strongly oxidizing conditions prior to burial. These results are consistent with other studies of paleosols where surface enrichment of organic carbon was observed [15,18,67,90]. However, it is possible that late diagenetic inputs of organics caused this enrichment, for example, by preferential flow and

716 accumulation in the paleosurface of each profile. Considering the Holocene radiocarbon dates for these
717 ~33 Ma paleosols (Table 1), results from this work cannot definitively rule out diagenesis as a mechanism
718 for surface enrichment, though it is unlikely that early and/or late diagenetic additions of organic carbon
719 could have preferentially accumulated in the near-surface horizons of these buried soils.
720
721 **3.5 Implications for Mars**
722 Recent work has considered putative paleosols on Mars as potential high priority environments
723 for *in-situ* analysis [29] and biosignature preservation [7]. This is because the composition and properties of
724 paleosols preserve evidence of paleoclimate, aqueous conditions, and life [7]. A major finding of this study
725 is that near-surface horizons of terrestrial paleosols appear to be a favorable location for SAM-EGA
726 detection of organic carbon. Like modern soils, the surface layers of Mars-analog paleosols examined
727 here show evidence of surface enrichment of organic carbon. Although the early diagenetic process of
728 burial decomposition of organic matter has likely reduced the organic carbon content of these ancient
729 soils by at least two orders of magnitude relative to modern soils [13], the enrichment of organic carbon in
730 surface horizons (~0.03 wt. %) and subsequent depletion in deeper layers (<0.01 wt. %) was readily
731 observable with SAM-EGA analog analysis.
732 Results from this study also have implications for interpreting the chemical and isotopic
733 biosignature preservation potential of Al and Fe smectite-bearing weathering profiles on Mars. However,
734 as discussed earlier, there are critical limitations to using terrestrial paleosols as analogs to interpret the
735 organic preservation potential of paleosols on Mars, such as major differences in the types and properties
736 of organic molecules deposited during soil formation. Irrevocable differences between Earth and Mars,
737 including climate and a complex terrestrial biosphere, preclude direct comparisons. In any case,
738 observations of refractory organic compounds that persist in terrestrial paleosols with Mars-like
739 mineralogy provides a reference frame for interpreting future observations of putative weathering profiles
740 on Mars. It is possible that clay minerals and/or amorphous phases in martian weathering profiles impart a
741 similar control on the fate of organic carbon.
742 Results from this work also provide an initial framework for investigation and sampling of
743 martian weathering profiles should they be encountered by current or future landed missions. Future *in-*
744 *situ* analysis of putative weathering profiles should begin at the surface and sample down the into the
745 unaltered protolith. However, if the entire profile is not accessible for investigation (e.g., outcrop is at a
746 topographic position inaccessible to the rover), the near-surface horizons of the profile, just below the
747 uppermost burial layer, should be considered the highest priority target for remote sensing, contact
748 science, and collection of a drilled sample for sample return to Earth.
749
750 **Conclusions**

751 The objectives of this study were a) to determine whether the organic carbon content of ~30-
752 million-year-old paleosols can be detected with a thermal and evolved gas analyzer configured to operate
753 like the SAM-EGA instrument onboard *Curiosity* Mars rover, and b) use radiocarbon (^{14}C) dating to
754 constrain the age of organic carbon in bulk paleosol samples. Radiocarbon dating of organic carbon in
755 four paleosol samples revealed the presence of recent and/or modern exogenous organic carbon. Samples
756 from 0 - 20 cm were dated to ~6,200 years BP and had a fraction modern (fM) value of ~0.4, while a
757 single deeper sample collected from 43 cm had a radiocarbon age of ~14,600 years BP and ~0.16 fM. The
758 presence of radiocarbon in paleosols could have resulted from the diagenetic addition of small amounts of

759   modern (< 1 Ka) organic carbon which mixed with ^{14}C-free endogenous organic carbon. Alternatively, a
760   diagenetic event between 6-14 Ka could have introduced exogenous organics, possibly through
761   groundwater alteration and/or precipitation-driven leaching of dissolved organic carbon. There may be a
762   sampling depth (e.g., > 1 meter into the outcrop) which decreases or eliminates organic additions from
763   exogenous sources. It is possible, however, that diagenesis has pervasively introduced exogenous organic
764   carbon to deeper samples. Holocene-age radiocarbon dates supported the hypothesis that paleosols from
765   the site contain exogenous organic carbon. These results highlight major challenges for determining the
766   source(s) and age of organic matter in terrestrial paleosols. Radiocarbon dating should be used in future
767   analog studies to help distinguish diagenetic organic inputs from original endogenous inputs.
768   SAM-EGA-like characterization of paleosols showed evolutions of CO, NO, CO_2, and organic
769   fragments. Coevolutions of CO_2 and organic fragments at ~400° C suggested the presence of refractory
770   organic carbon. However, like other oxidized terrestrial paleosols of Cenozoic age and older, only trace
771   amounts (<0.1 wt. %) of organic carbon was detected, which most likely was a result of diagenetic
772   decomposition of organic matter over geological time scales. Many samples examined in this work
773   typically contained very low amounts (~0.01 wt. %) of organic carbon, but these low values were
774   nevertheless detectable by SAM-like evolved gas analysis of bulk samples. These results suggest the
775   organic fraction of potential martian weathering profiles may be detectable with evolved gas analysis,
776   even if organic concentrations are low.
777   A major result of this work was that organic carbon was concentrated in near-surface horizons of
778   paleosols while deeper horizons were depleted in organic carbon. Like modern soils, these ancient soils
779   were enriched in organic carbon in near-surface horizons, and it appears that this trend persisted in these
780   samples despite burial decomposition of organic carbon over geological time scales. Alternatively,
781   diagenesis could have pervasively introduced exogenous organic carbon, but it is unlikely such organic
782   contamination would preferentially accumulate in the surface layers of each successive buried soil profile.
783   Surface enrichment of organic carbon in possible weathering profiles on Mars may therefore constitute a
784   putative chemical biosignature. This work demonstrates that analytical techniques similar to SAM-EGA
785   can detect trace amounts of organic carbon in complex pedogenic mineral matrices. The search for past
786   life on ancient land surfaces of Mars should include targeting Martian weathering profiles for *in-situ*
787   biosignature investigation and Mars Sample Return.
788
789   **Additional Information**
790
800
801   **Author Contribution Statement**

802 A.P.B and J.V.C designed the study, performed all laboratory analyses and drafted the manuscript. J.V.C,
803 D.W.M, P.D.A, and B.S contributed to data analysis and interpretation. B.H.H identified similarities
804 between Mars and John Day paleosols and assisted with fieldwork and data interpretation. L.C.R.S
805 provided radiocarbon analyses and interpreted the data. J.V.C, P.D.A, B.S, D.W.M, and L.C.R.S
806 supervised the project. A.P.B drafted all figures. All authors contributed to the manuscript.
807
808 **Author Disclosure Statement**

809 No competing financial interests exist.

810 **Supplementary data is available online at:**
811

812 **4   References**

813 1.   Retallack, G. J. *Soil of the Past*. (Wiley Blackwell, 2019).

814 2.   Liu, J., Michalski, J. R. & Zhou, M. Intense subaerial weathering of eolian sediments in
815   Gale crater, Mars. *Sci. Adv.* **7**, (2021).

816 3.   Carter, J., Loizeau, D., Mangold, N., Poulet, F. & Bibring, J. Widespread surface
817   weathering on early Mars : A case for a warmer and wetter climate. *Icarus* **248**, 373–382
818   (2015).

819 4.   Loizeau, D. *et al.* Quantifying widespread aqueous surface weathering on Mars : The
820   plateaus south of Coprates Chasma. *Icarus* **302**, 451–469 (2018).

821 5.   Bishop, J. L. *et al.* Surface clay formation during short-term warmer and wetter conditions
822   on a largely cold ancient Mars. *Nat. Astron.* **2**, 206–213 (2018).

823 6.   Liu, J. *et al.* Anoxic chemical weathering under a reducing greenhouse on early Mars. *Nat.*
824   *as* (2021) doi:https://doi.org/10.1038/s41550-021-01303-5.

825 7.   Bishop, J. L. *et al.* Potential high priority subaerial environments for Mars sample return.
826   *Proc. Second Int. Mars Sample Return Conf.* **2071**, (2018).

827 8.   Beaty, D. W. *et al.* The potential science and engineering value of samples delivered to
828   Earth by Mars sample return. *Meteorit. Planet. Sci.* **671**, 667–671 (2019).

829 9.   Horgan, B. Strategies for Searching for Biosignatures in Ancient Martian Sub-Aerial
830   Surface Environments. *Biosignature Preserv. Detect. Mars Analog Environ.* 7463 (2016)
831   doi:10.1089/ast.2016.1627.

832 10. Raynaud, X. & Nunan, N. Spatial ecology of bacteria at the microscale in soil. *PLoS One*
833   **9**, (2014).

834 11. Lehmann, J. & Kleber, M. The contentious nature of soil organic matter. *Nature* 1–9
835   (2015) doi:10.1038/nature16069.

836 12. Dynarski, K. A., Bossio, D. A. & Scow, K. M. Dynamic Stability of Soil Carbon:
837   Reassessing the "Permanence" of Soil Carbon Sequestration. *Front. Environ. Sci.* **8**,
838   (2020).

839 13. Broz, A. P. Organic Matter Preservation in Ancient Soils of Earth and Mars. *Life* **10**,
840   (2020).

841 14. Matthewman, R., Cotton, L. J., Martins, Z. & Sephton, M. A. Organic geochemistry of
842   late Jurassic paleosols (Dirt Beds) of Dorset , UK. *Mar. Pet. Geol.* **37**, 41–52 (2012).

843 15. Liivamägi, S. *et al.* Paleosols on the Ediacaran basalts of the East European Craton: a
844   unique record of paleoweathering with minimum diagenetic overprint. *Precambrian Res.*
845   (2018) doi:10.1016/j.precamres.2018.07.020.

846 16. Kremer, B., Kaźmierczak, J. & Środoń, J. Cyanobacterial-algal crusts from Late Ediacaran
847   paleosols of the East European Craton. *Precambrian Res.* (2017)
848   doi:10.1016/j.precamres.2017.12.018.

849 17. Watanabe, Y., Martin, J. E. . & Ohmoto, H. Geochemical evidence for terrestrial
850   ecosystems 2.6 billion years ago. *Nature* **408**, (2000).

851 18. Rye, R. & Holland, H. Life associated with a 2 . 76 Ga ephemeral pond ?: Evidence from
852   Mount Roe # 2 paleosol. *Geology* **28**, 483–486 (2000).

853 19. Retallack, G. J. & Mao, X. Paleoproterozoic (ca . 1 . 9 Ga) megascopic life on land in
854   Western Australia. *Palaeogeogr. Palaeoclimatol. Palaeoecol.* **532**, 109266 (2019).

855 20. Retallack, G. J. & Krull, E. S. Landscape ecological shift at the Permian – Triassic
856   boundary in Antarctica. *Aust. J. Earth Sci.* **46**, 785–812 (1999).

857 21. Krull, E. S. & Retallack, G. J. 13C depth profiles from paleosols across the Permian-
858   Triassic boundary : Evidence for methane release. *GSA Bull.* **112**, 1459–1472 (2000).

859 22. Bestland, E. . Alluvial Terraces and Paleosols As Indicators Of Early Oligocene Climate
860   Change (John-Day Formation, Oregon). *J. Sediment. Res.* **67**, 840–855 (1997).

861 23. Retallack, G. J., Bestland, E. . & Fremd, T. . Eocene and Oligocene Paleosols of Central
862   Oregon. *Geol. Soc. Am. Spec. Pap.* **344**, 1–192 (2000).

863 24. Horgan, B., Bishop, L., Christensen, P. R. & Bell, J. F. Potential ancient soils preserved at
864   Mawrth Vallis from comparisons with Eastern Oregon paleosols: Implications for Early
865   Martian Climate. *Third Conf. Early Mars* **7074**, 12–13 (2012).

866 25. Smith, R. ., Horgan, B., Rampe, E. & Dehouck, E. The Composition of Amorphous
867   Phases in Soils and Sediments on Earth and Mars. *49th Lunar Planet. Sci. Conf. 2018* 14–
868   15 (2018).

869 26. Horgan, B., Rutledge, A. & Rampe, E. . Clay mineralogy and crystallinity as a climatic
870   indicator: Evidence for both cold and temperate conditons on early Mars. *46th Lunar
871   Planet. Sci. Conf.* 3–4 (2018) doi:10.1029/2006.

872 27. Bestland, E. A. Fossil Andisols identified with mass-balance geochemistry (Oligocene
873   John Day Formation, Oregon, U.S.A.). *J. Sediment. Res.* **72**, 673–686 (2002).

874 28. Sheldon, N. D., Retallack, G. J. & Tanaka, S. Geochemical Climofunctions from North
875   American Soils and Application to Paleosols across the Eocene - Oligocene Boundary in
876   Oregon Geochemical Climofunctions from North American Soils and Application to
877   Paleosols across the Eocene-Oligocene Boundary in Or. *J. Geol.* **110**, 687–696 (2015).

878 29. Hays, L. E. *et al.* Biosignature Preservation and Detection in Mars Analog Environments.
879   *Astrobiology* **17**, 363–400 (2017).

880 30. Smith, R. J., Rampe, E. B., Horgan, B. H. N. & Dehouck, E. Deriving Amorphous
881   Component Abundance and Composition of Rocks and Sediments on Earth and Mars. *J.*

882   *Geophys. Res. Planets* **123**, 2485–2505 (2018).

883   31.   Poulet, F. *et al.* Mawrth Vallis, Mars: A Fascinating Place for Future In Situ Exploration.
884   *Astrobiology* **20**, 1–36 (2020).

885   32.   Viviano-Beck, C. E. *et al.* Revised CRISM spectral parameters and summary products
886   based on the currently detected mineral diversity on Mars. *J. Geophys. Res. Planets* **119**,
887   1403–1431 (2014).

888   33.   Bishop, J. L. *et al.* Multiple mineral horizons in layered outcrops at Mawrth Vallis, Mars,
889   signify changing geochemical environments on early Mars. *Icarus* **341**, 113634 (2020).

890   34.   Lantz, C. *et al.* Planetary Terrestrial Analogues Library project: 1. characterization of
891   samples by near-infrared point spectrometer. *Planet. Space Sci.* **189**, 104989 (2020).

892   35.   Smith, R. . & Horgan, B. H. N. Nanoscale Variations in Natural Amorphous and
893   Nanocrystalline Weathering Products in Mafic to Intermediate Volcanic Terrains on
894   Earth : Implications for Amorphous Detections on Mars. *J. Geophys. Res. Planets* **126**, 1–
895   30 (2021).

896   36.   Horgan, B. H. N. Climate change and a sequence of habitable ancient surface
897   environments preserved in pedogenically altered sediments at Mawrth Vallis, Mars. in
898   *Lunar and Planetary Science Conference* 3059 (2013).

899   37.   Loizeau, D. *et al.* History of the clay-rich unit at Mawrth Vallis, Mars: High- resolution
900   mapping of a candidate landing site. *J. Geophys. Res. Planets* 1820–1846 (2015)
901   doi:10.1002/2015JE004894.Received.

902   38.   Danielson, J. . *et al.* Characterization of outcrops containing 'doublet' spectra at Mawrth
903   Vallis, Mars. *Lunar Planet. Sci. Conf.* **2019**, 1–179 (2019).

904   39.   Noe Dobrea, E. Z. *et al.* Characterizing the mechanisms for the preservation of organics at
905   the Painted Desert: Lessons for MSL, Exo-Mars, and Mars 2020. *47th Lunar Planet. Sci.*
906   *Conf.* Abstract #2796 (2016).

907   40.   Bishop, J. L. & Rampe, E. B. Evidence for a changing Martian climate from the
908   mineralogy at Mawrth Vallis. *Earth Planet. Sci. Lett.* **448**, 42–48 (2016).

909   41.   Horgan, B. H. N., Anderson, R. B., Dromart, G., Amador, E. S. & Rice, M. S. The mineral
910   diversity of Jezero crater : Evidence for possible lacustrine carbonates on Mars. *Icarus*
911   **339**, 113526 (2020).

912   42.   Mahaffy, P. R. *et al.* The sample analysis at mars investigation and instrument suite.
913   *Space Sci. Rev.* **170**, 401–478 (2012).

914   43.   Eigenbrode, J. L. *et al.* Organic matter preserved in 3-billion-year-old mudstones at Gale
915   crater, Mars. *Science (80-.).* **360**, 1096–1101 (2018).

916   44.   Szopa, C. *et al.* First Detections of Dichlorobenzene Isomers and Trichloromethylpropane
917   from Organic Matter Indigenous to Mars Mudstone in Gale Crater , Mars : Results from
918   the Sample Analysis at Mars Instrument Onboard the Curiosity Rover. **20**, 292–306
919   (2020).

920   45.   Archer, P. . *et al.* Abundances and implications of volatile-bearing species from evolved
921   gas analysis of the Rocknest aeolian deposit, Gale Crater, Mars. *J. Geophys. Res. Planets*
922   237–254 (2014) doi:10.1002/2013JE004493.Received.

923 46. Ming, D. W. *et al.* Volatile and Organic Compositions of Sedimentary Rocks in
924 Yellowknife Bay , Gale Crater , Mars. *Sci. Express* 1–15 (2014)
925 doi:10.1126/science.1245267.

926 47. Freissinet, C. *et al.* Organic molecules in the Sheepbed Mudstone, Gale Crater, Mars. *J.*
927 *Geophys. Res. Planets* **120**, 495–514 (2015).

928 48. Mcadam, A. C. *et al.* Constraints on the Mineralogy and Geochemistry of Vera Rubin
929 Ridge , Gale Crater , Mars , From Mars Science Laboratory Sample Analysis at Mars
930 Evolved Gas Analyses. *J. Geophys. Res. Planets* 1–26 (2020)
931 doi:10.1029/2019JE006309.

932 49. Goesmann, F. *et al.* The Mars Organic Molecule Analyzer (MOMA) Instrument:
933 Characterization of Organic Material in Martian Sediments. *Astrobiology* **17**, 655–685
934 (2017).

935 50. Ivanov, M. A., Slyuta, E. N., Grishakina, E. A. & Dmitrovskii, A. A. Geomorphological
936 Analysis of ExoMars Candidate Landing Site Oxia Planum. *Sol. Syst. Res.* **54**, 1–14
937 (2020).

938 51. Loizeau, D. *et al.* ExoMars 2020 Surface Mission: Choosoing a Landing Site. **2019**, 2019–
939 2020 (2020).

940 52. Rampe, E. . *et al.* Amorphous phases on the surface of Mars. *Eighth Int. Conf. Mars* 1–2
941 (2014).

942 53. Fornaro, T., Steele, A. & Brucato, J. R. Catalytic/protective properties of martian minerals
943 and implications for possible origin of life on mars. *Life* **8**, 1–41 (2018).

944 54. Lewis, J. M. T. *et al.* Pyrolysis of Oxalate, Acetate, and Perchlorate Mixtures and the
945 Implications for Organic Salts on Mars. *J. Geophys. Res. Planets* **126**, (2021).

946 55. Nelson, P. N. & Baldock, J. A. Estimating the molecular composition of a diverse range of
947 natural organic materials from solid-state C NMR and elemental analyses.
948 *Biogeochemistry* **72**, 1–34 (2005).

949 56. Williams, E. K., Fogel, M. L., Berhe, A. A. & Plante, A. F. Distinct bioenergetic
950 signatures in particulate versus mineral-associated soil organic matter. *Geoderma* **330**,
951 107–116 (2018).

952 57. Marin-Spiotta, E. *et al.* Long-term stabilization of deep soil carbon by fire and burial
953 during early Holocene climate change. *Nat. Geosci.* **7**, 428–432 (2014).

954 58. Otto, A., Shunthirasingham, C. & Simpson, M. J. A comparison of plant and microbial
955 biomarkers in grassland soils from the Prairie Ecozone of Canada. *Org. Geochem.* **36**,
956 425–448 (2005).

957 59. Plante, A. F., Fernández, J. M., Haddix, M. L., Steinweg, J. M. & Conant, R. T.
958 Biological, chemical and thermal indices of soil organic matter stability in four grassland
959 soils. *Soil Biol. Biochem.* **43**, 1051–1058 (2011).

960 60. Bishop, J. L. *et al.* What the ancient phyllosilicates at Mawrth Vallis can tell us about
961 possible habitability on early Mars. *Planet. Space Sci.* **86**, 130–149 (2013).

962 61. Homann, M. *et al.* Microbial life and biogeochemical cycling on land 3,220 million years
963 ago. *Nat. Geosci.* **11**, 665–671 (2018).

964   62.   Finke, N. *et al.* Mesophilic microorganisms build terrestrial mats analogous to
965   Precambrian microbial jungles. *Nat. Commun.* **10**, 1–11 (2019).

966   63.   Retallack, G. J. Astropedology: palaeosols and the origins of life. *Geol. Today* **32**, 172–
967   178 (2016).

968   64.   Retallack, G. J. & Noffke, N. Are there ancient soils in the 3 . 7 Ga Isua Greenstone Belt ,
969   Greenland ? *Palaeogeogr. Palaeoclimatol. Palaeoecol.* **514**, 18–30 (2019).

970   65.   Nabhan, S., Wiedenbeck, M., Milke, R. & Heubeck, C. Biogenic overgrowth on detrital
971   pyrite in ca. 3.2 Ga Archean paleosols. *Geology* **44**, 763–766 (2016).

972   66.   Gay, A. . & Grandstaff, D. E. Chemistry and mineralogy of precambrian paleosols at elliot
973   lake, ontario, canada. *Precambrian Res.* **12**, 349–373 (1980).

974   67.   Watanabe, Y., Stewart, B. W. & Ohmoto, H. Organic- and carbonate-rich soil formation
975   ~2.6 billion years ago at Schagen, East Transvaal district, South Africa. *Geochim.*
976   *Cosmochim. Acta* **68**, 2129–2151 (2004).

977   68.   Ramirez, R. M. *et al.* Warming early Mars with CO2 and H2. *Nat. Geosci.* **7**, 59–63
978   (2014).

979   69.   Apesteguia, M., Plante, A. F. & Virto, I. Methods assessment for organic and inorganic
980   carbon quantification in calcareous soils of the Mediterranean region. *Geoderma Reg.* **12**,
981   39–48 (2018).

982   70.   Schiller, M., Dickinson, W., Ditchburn, R. G., Graham, I. J. & Zondervan, A.
983   Atmospheric 10 Be in an Antarctic soil: Implications for climate change . *J. Geophys. Res.*
984   **114**, 1–8 (2009).

985   71.   Balco, G., Stone, J. O. H. & Mason, J. A. Numerical ages for Plio-Pleistocene glacial
986   sediment sequences by Al / 10 Be dating of quartz in buried paleosols. *Earth Planet. Sci.*
987   *Lett.* **232**, 179–191 (2005).

988   72.   Sweeney, K. E., Roering, J. J. & Ellis, C. Experimental evidence for hillslope control of
989   landscape scale. *Science (80-.).* **349**, 51–53 (2015).

990   73.   Lawrence, C. R., Schulz, M. S., Masiello, C. A., Chadwick, O. A. & Harden, J. W. The
991   trajectory of soil development and its relationship to soil carbon dynamics. *Geoderma*
992   **403**, (2021).

993   74.   Ewing, S. A., Macalady, J. L., Warren-Rhodes, K., McKay, C. P. & Amundson, R.
994   Changes in the soil C cycle at the arid-hyperarid transition in the Atacama Desert. *J.*
995   *Geophys. Res.* **113**, 1–16 (2008).

996   75.   Sutter, B. *et al.* Evolved gas analyses of sedimentary rocks and eolian sediment in Gale
997   Crater, Mars: Results of the Curiosity rover's sample analysis at Mars instrument from
998   Yellowknife Bay to the Namib Dune. *J. Geophys. Res. Planets* 2574–2609 (2017)
999   doi:10.1002/2016JE005225.

1000   76.   Cannon, K. M., Sutter, B., Ming, D. W., Boynton, W. V. & Quinn, R. Perchlorate induced
1001   low temperature carbonate decomposition in the Mars Phoenix Thermal and Evolved Gas
1002   Analyzer (TEGA). *Geophys. Res. Lett.* **39**, 2–6 (2012).

1003   77.   Sutter, B. *et al.* The detection of carbonate in the martian soil at the Phoenix Landing site:
1004   A laboratory investigation and comparison with the Thermal and Evolved Gas Analyzer

1005   (TEGA) data. *Icarus* **218**, 290–296 (2012).

1006   78.   Stern, J. C. *et al.* Evidence for indigenous nitrogen in sedimentary and aeolian deposits
1007   from the Curiosity rover investigations at Gale ... *PNAS* (2015)
1008   doi:10.1073/pnas.1420932112.

1009   79.   Kurth, V. J., MacKenzie, M. D. & DeLuca, T. H. Estimating charcoal content in forest
1010   mineral soils. *Geoderma* **137**, 135–139 (2006).

1011   80.   De la Rosa, J. M. *et al.* Use of pyrolysis/GC-MS combined with thermal analysis to
1012   monitor C and N changes in soil organic matter from a Mediterranean fire affected forest.
1013   *Catena* **74**, 296–303 (2008).

1014   81.   Miller, K. B., McCahon, T. J. & West, R. R. Lower Permian (wolfcampian) paleosol-
1015   bearing cycles of the U.S. Midcontinent: Evidence of climatic cyclicity. *Journal of
1016   Sedimentary Research* vol. 66 71–84 (1996).

1017   82.   Kleber, M., Mikutta, R., Torn, M. . & Jahn, R. Poorly crystalline mineral phases protect
1018   organic matter in acid subsoil horizons. *Eur. J. Soil Sci.* 717–725 (2005)
1019   doi:10.1111/j.1365-2389.2005.00706.x.

1020   83.   Schmidt, M. W. I. *et al.* Persistence of soil organic matter as an ecosystem property.
1021   *Nature* (2011) doi:10.1038/nature10386.

1022   84.   Kleber, M. *et al.* Dynamic interactions at the mineral–organic matter interface. *Nat. Rev.
1023   Earth Environ.* **2**, 402–421 (2021).

1024   85.   François, P. *et al.* Magnesium sulfate as a key mineral for the detection of organic
1025   molecules on Mars using pyrolysis. *J. Geophys. Res. – Planets* 61–74 (2015)
1026   doi:10.1002/2015JE004884.Received.

1027   86.   Reardon, P. N. *et al.* Abiotic Protein Fragmentation by Manganese Oxide: Implications for
1028   a Mechanism to Supply Soil Biota with Oligopeptides. *Environ. Sci. Technol.* **50**, 3486–
1029   3493 (2016).

1030   87.   Alekseeva, T. V, Zolotareva, B. N. & Kolyagin, Y. G. Nonhydrolyzable Part of Soil
1031   Organic Matter in Buried and Modern Soils. *Eurasian Soil Sci.* **52**, 632–643 (2019).

1032   88.   Mcadam, A. ., Sutter, B., Archer, P. ., Franz, H. . & Eigenbrode, J. . The chemistry and
1033   mineralogy of the Glen Torridon clay-bearing unit from Mars Science Laboratory Sample
1034   Analysis at Mars. *51st Lunar Planet. Sci. Conf.* **2243**, 60–74 (2020).

1035   89.   PiPujol, M. D. & Buurman, P. The distinction between ground-water gley and surface-
1036   water gley phenomena in Tertiary paleosols of the Ebro basin, NE Spain. *Palaeogeogr.
1037   Palaeoclimatol. Palaeoecol.* **110**, 103–113 (1994).

1038   90.   Liu, J. *et al.* Reflectance spectroscopy applied to clay mineralogy and alteration intensity
1039   of a thick basaltic weathering sequence in Hainan Island , South China. *Appl. Clay Sci.*
1040   105923 (2020) doi:10.1016/j.clay.2020.105923.

1041

1042